

# The steady-state population of Earth's co-orbitals of lunar provenance

Elisa Maria Alessi<sup>a</sup>, Robert Jedicke<sup>b</sup>

<sup>a</sup>*Istituto di Matematica Applicata e Tecnologie Informatiche, Consiglio Nazionale delle Ricerche (IMATI-CNR), Via Alfonso Corti 12, 20133 Milano, Italy. [elisamaria.alessi@cnr.it](mailto:elisamaria.alessi@cnr.it)*

<sup>b</sup>*Institute for Astronomy, University of Hawai'i, 2680 Woodlawn Drive, Honolulu, HI 96822, USA. [jedicke@hawaii.edu](mailto:jedicke@hawaii.edu)*

---

## Abstract

The population of natural objects in a 1:1 mean motion resonance with Earth are known as Earth's co-orbitals. Main belt objects can dynamically evolve into Earth co-orbitals but taxonomic studies of some of them have suggested that they are more likely to be lunar material. While it has long been known that lunar ejecta can achieve Earth co-orbital status, in this work we calculate their expected steady-state size-frequency distribution from the impact rate of asteroids and comets on the Moon's surface, the ejecta's size-frequency and speed distribution, and dynamical integration of the particles for millions of years, among other factors. We also classify known and synthetic co-orbitals by their regime (quasi-satellite, horseshoe, tadpole, or compound) and compute the probability of transitions between them. Our nominal solution predicts that there are  $\gtrsim 70$  Earth co-orbitals in the steady-state population larger than 10 m in diameter with a lunar provenance but there are orders-of-magnitude systematic uncertainty on the value. We used NEOMOD3 to calculate that about 1600 are expected in the co-orbital population with a main belt provenance and they have higher eccentricity and inclination than those from the Moon. New taxonomic classifications for more Earth co-orbitals will reduce the uncertainties on e.g. crater scaling relations that will, in turn, reduce the uncertainties in the calculation of the steady-state population of Earth's co-orbitals with a lunar origin. The mineralogy and abundance of Earth's co-orbitals is also of interest to commercial asteroid mining ventures because they are the lowest  $\Delta v$  targets in the asteroid population.

*Keywords:*

---

## 1. Introduction

When two objects orbit a primary body in the same amount of time, i.e. have nearly identical semi-major axes, they are in a 1:1 mean motion resonance (MMR), or *co-orbital motion*, like Jupiter's Trojans and some moons, e.g. Janus and Epimetheus (Morais and Morbidelli, 2002). The Earth is accompanied by several known co-orbitals, the first one identified as such being (3753) Cruithne (Wiegert et al., 1997), and including amongst its members (469219) Kamo'oalewa, the target of the China National Space Administration's

Tianwen-2 spacecraft mission (e.g. Zhang et al., 2025). Dynamical integration of main belt objects into the inner solar system suggest that co-orbitals can be supplied by the main belt (e.g. Granvik et al., 2018; Nesvorný et al., 2024) but the colors and spectra of several co-orbitals are more consistent with lunar material (e.g. Bolin et al., 2020; Sharkey et al., 2021; Kareta et al., 2025). Thus, while it has long been known that lunar ejecta can become co-orbital, in this work we calculate the expected steady-state size-frequency distribution of Earth’s co-orbitals of lunar provenance.

Co-orbitals can be classified into three regimes in the prograde quasi-planar scenario: tadpole, horseshoe, and quasi-satellite. In the framework of the circular restricted three-body problem (CR3B), tadpole orbits are Lyapunov-stable, stemming from the  $L_4$  and  $L_5$  equilibrium points, and quasi-periodic in their neighborhood (e.g. Szebehely, 1967; Gómez et al., 2001), horseshoe orbits correspond to the hyperbolic invariant manifold of the  $L_3$  point and to families of stable and unstable periodic and quasi-periodic orbits in its neighborhood (Barrabés and Mikkola, 2005; Barrabés and Ollé, 2006), and quasi-satellite orbits appear to orbit the planet, the secondary body, in a retrograde manner.

The tadpole regime has been studied extensively, especially in the framework of the Trojan asteroids of the Sun-Jupiter system (e.g. Mikkola et al., 1994; Robutel et al., 2005; Hui et al., 2021; Li et al., 2023; Greenstreet et al., 2024). Every planet in our solar system except Mercury (e.g. Christou, 2013; Polishook et al., 2017; Scholl et al., 2005; Hui et al., 2024; de la Fuente Marcos and de la Fuente Marcos, 2017; Nesvorný and Vokrouhlický, 2009) has at least one associated Trojan asteroid and Earth has two, 2010 TK<sub>7</sub> and 2020 XL<sub>5</sub> (Hui et al., 2021; Santana-Ros, et al., 2022).

The quasi-satellite family of periodic and quasi-periodic orbits is of interest because it arises in correspondence with the ‘f’ family of periodic orbits in the Strömgen classification (Strömgen, 1933), what Poincaré called ‘a family of the first kind’ (Szebehely, 1967). This means that we can generate the first orbit of the family starting from a circular periodic orbit in the Keplerian approximation and perturb it by introducing a secondary massive body into the system. The additional source of gravity does not change the stability of the family of periodic orbits (cf. Mikkola and Innanen, 1997; Pousse et al., 2017; Jorba-Cuscó and Epenoy, 2021, and references therein). The quasi-satellites can be sub-classified in three domains: heliocentric, planetocentric, and ‘limbo’, for which both the Sun and the planet are important and none of them can be treated as a perturbation (Pousse et al., 2017; Voyatzis and Antoniadou, 2018). In this study, we investigate heliocentric quasi-satellite dynamics, although the data analyzed were derived from trajectories residing in the transitional (‘limbo’) regime. Quasi-satellite orbits have been studied in the context of the motion of asteroids and satellites (e.g. Mikkola et al., 2004; Kinoshita and Nakai, 2007; Wajer, 2010; de la Fuente Marcos and de la Fuente Marcos, 2012) and for mission design (e.g. Ogawa et al., 2019; Jorba-Cuscó and Epenoy, 2021; Lavagna et al., 2024; Cicalò et al., 2025). Pousse et al. (2017) provides a comprehensive review of quasi-satellite orbits and their treatment.

Horseshoe trajectories were first considered by Brown (1911) in an approximation of the planar CR3B problem. Later, some orbits and families of orbits of this kind were numerically identified in the Sun–Jupiter system (Rabe, 1961), followed by numerous others in the general

three-body problem (e.g. [Llibre and Ollé, 2001](#); [Barrabés and Ollé, 2006](#); [Bengochea et al., 2013](#)). Several analytical theories have been developed to describe the long-term dynamics of horseshoe orbits in the three-body problem, mainly in the case of the Janus–Epimetheus co-orbital pair (e.g. [Dermott and Murray, 1981](#); [Yoder et al., 1983](#); [Spirig and Waldvogel, 1985](#); [Robutel and Pousse, 2013](#); [Cors et al., 2019](#)).

Objects in co-orbital motion can experience transitions between regimes due to the orbits having non-negligible inclinations or to  $n$ -body interactions (cf. [Namouni, 1999](#); [Christou, 2000](#)). Earth’s co-orbitals are also the proximal source region of Earth’s ‘minimoons’ as they are the only objects that can energetically be captured in the Earth-Moon system ([Granvik et al., 2012](#)).

Among the known co-orbitals, (469219) Kamo‘oalewais particularly noteworthy. With an absolute magnitude<sup>1</sup> of  $H = 24.3$ , it is estimated to have a diameter<sup>1</sup> in the range from 24 m to 107 m, and its orbit undergoes transitions between the horseshoe and quasi-satellite regimes. Spectroscopic studies ([Sharkey et al., 2021](#)) indicate that it may have a lunar origin which has motivated a series of dynamical studies to evaluate the possibility that lunar ejecta become co-orbitals ([Castro-Cisneros et al., 2023](#); [Jiao et al., 2024](#); [Sfair et al., 2025](#); [Zhu et al., 2025](#)). Indeed, [Jiao et al. \(2024\)](#) suggest that they have traced its origin to the Giordano Bruno crater, a 1–10 Myr old and  $\sim 22$  km diameter crater (e.g. [Morota et al., 2009](#)). That origin story was subsequently studied by [Fenucci et al. \(2026\)](#) who claim that it is unlikely that (469219) Kamo‘oalewa was ejected from Giordano Bruno. In any event, this hypothesis will be tested *in-situ* by the Tianwen-2 spacecraft which was launched in May 2025 and will arrive at (469219) Kamo‘oalewain the summer of 2026 ([Zhang et al., 2021](#)).

Two other Earth co-orbitals have also been spectroscopically associated with lunar ejecta: the decameter-scale 2024 PT<sub>5</sub> ([Bolin et al., 2025a](#); [Kareta et al., 2025](#)) and the meter-scale 2020 CD<sub>3</sub> ([Bolin et al., 2020](#)). Both objects had a negative binding energy with Earth but only 2020 CD<sub>3</sub> satisfied the conditions to be informally classified as a ‘minimoon’ ([Fedorets et al., 2017](#)). Intriguingly, backwards propagation of 2020 CD<sub>3</sub>’s trajectory suggests that it had a 1.4% chance of intersecting the lunar surface in September of 2017, at the time it was captured into its geocentric orbit. This suggests that it might have been ejected by an impact at that time but [Fedorets et al. \(2020\)](#) rejected that argument for a number of reasons. Even so, it may have been ejected in an impact long ago and remained in, or near, Earth co-orbital space to be captured again in 2017.

While it has long been known that lunar ejecta *can* evolve onto Earth-like orbits, how often does it happen and what fraction of the steady-state co-orbital population has a lunar provenance? For instance, the near-Earth object model NEOMOD3 predicts that there are 44 objects of main belt origin with an orbit and absolute magnitude similar to (469219) Kamo‘oalewa, i.e. with  $H < 27$ ,  $0.05 \leq e \leq 0.15$ , and  $5^\circ \leq i \leq 15^\circ$ . The largest known Earth co-orbital is the  $\sim 3000$  m diameter<sup>2</sup> (3753) Cruithne and it seems unlikely that an object of that size could be liberated from the Moon’s surface by an asteroid impact with sufficient speed to escape the Earth-Moon system, transition into an Earth-like orbit,

---

<sup>1</sup>[https://ssd.jpl.nasa.gov/tools/sbdb\\_lookup.html#/?sstr=469219](https://ssd.jpl.nasa.gov/tools/sbdb_lookup.html#/?sstr=469219)

<sup>2</sup>Assuming an albedo of 0.143 that assigns an  $H = 17.75$  object a diameter of 1 km.

and remain there long enough to be identified in a co-orbital state at this time, given that the dynamical lifetime of objects in near-Earth space is on the order of millions of years (e.g. Gladman et al., 1997).

In addition to the scientific merits of understanding the provenance of objects in the inner solar system, the Earth’s co-orbitals are some of the lowest  $\Delta v$  mission targets (e.g. Granvik et al., 2013; Jedicke et al., 2018). They are thus interesting targets for space exploration as the solar system’s dynamics have performed the task of transporting objects from the Moon and main belt into more easily accessible orbits. Their economic and strategic viability will also depend on their mineralogy which is different for the two sources.

## 2. Method

### 2.1. Co-orbital dynamics

The integrations for this work were performed by Jedicke et al. (2025) who calculated the steady-state size-frequency and orbital element distribution of minimoons generated by lunar impacts. We used the results of their integrations during the time periods in which the particles were in heliocentric orbit.

We refer the reader to Jedicke et al. (2025) for the details of their simulation and only provide a high level summary here. Their work simulated the fate of 12,000 particles launched from 100 random locations on the Moon’s surface at 19 different speeds, 6 azimuth angles, and 45° elevation angle. The particles were launched at evenly spaced times within a Metonic cycle of  $\sim 19$  yr and integrated using REBOUND (Rein and Liu, 2012) with the 10 most massive solar system objects as perturbers. The particles were integrated for up to 55 Myr or until they left a torus enveloping Earth’s orbit.

The state of each particle during a heliocentric phase was recorded every 7,500 days,  $\sim 20.5$  yr, including the heliocentric orbital elements and resonant angle with the ecliptic as the reference plane. The time step was selected to allow the identification of co-orbital behavior while also considering data storage limitations. Particles typically remain in the horseshoe and tadpole states for hundreds of years, whereas quasi-satellite states persist only for a few decades (e.g. Di Ruzza et al., 2023; Cortese et al., 2025).

Earlier studies of the dynamical evolution of ejected lunar material were similar to this work but differed in the details of their assumptions and focus (e.g. Castro-Cisneros et al., 2023; Jiao et al., 2024; Zhu et al., 2025; Sfair et al., 2025). The most recent studies typically employed the REBOUND integrator that was used here but with different sets of perturbers. The propagation intervals and time steps were both shorter and longer than ours. Some of the studies specifically examined ejecta from the Giordano Bruno crater while others used random locations on the lunar surface. Our study used the largest number of launch speeds although some of the others considered a wider range. While the different studies differ in their details the integrations tend to be insensitive to some of the initial conditions. For instance, Sfair et al. (2025) showed that their results were unaffected by both the altitude and azimuth of the ensemble of particles’s launch from the lunar surface and Zhu et al. (2025) state that ‘the orbital dynamics of escaping ejecta are largely insensitive to the launch positions and angles’.

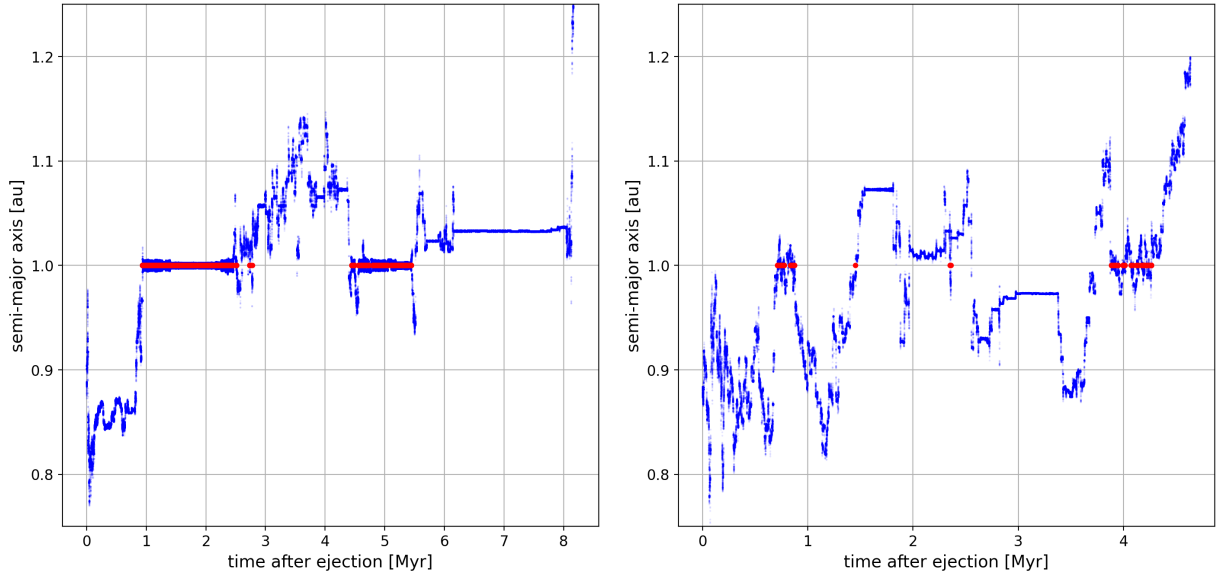


Figure 1: (blue) Semi-major axis time series highlighting (red) candidate co-orbital intervals for two test particles.

We identified the particles’ co-orbital regimes and time periods based on the software developed by [Di Ruzza et al. \(2023\)](#) extended with the techniques developed in [Cortese et al. \(2025\)](#). The first step was to identify co-orbital candidates by pinpointing times at which a particle’s semi-major axis crossed  $a = 1$  au and consider the time intervals during which the variation in semi-major axis is  $\leq 3\%$  (fig. 1).

The regimes were then distinguished by the behavior of the resonant angle,  $\theta$ , the difference between the longitudes of the asteroid,  $L$ , and Earth,  $L_E$ ,

$$\theta = L - L_E = (\Omega + \omega + M) - (\Omega_E + \omega_E + M_E), \quad (1)$$

where the  $E$  subscript refers to the orbital elements of Earth, the parameters without subscripts refer to the particle,  $\Omega$  is the longitude of the ascending node,  $\omega$  is the argument of pericenter, and  $M$  is the mean anomaly.

Following [Pousse and Alessi \(2022\)](#) and [Cortese et al. \(2025\)](#) the co-orbital regimes are formally defined as

- *Quasi-satellite* (QS): when  $\theta$  oscillates around  $0^\circ$  (fig. 2);
- *Tadpole* (TP): when  $\theta$  oscillates around  $\pm 60^\circ$  (fig. 3);
- *Horseshoe* (HS): when  $\theta$  oscillates around  $180^\circ$  (fig. 4);
- *Compound* (CP): when  $\theta$  oscillates around  $180^\circ$  but, as a combination of the horseshoe and quasi-satellite regimes,  $\theta$  crosses  $0^\circ$  (fig. 5). The CP regime is different from a transition between a horseshoe and a quasi-satellite regime as experienced by Kamo’oalewa (fig. 6).

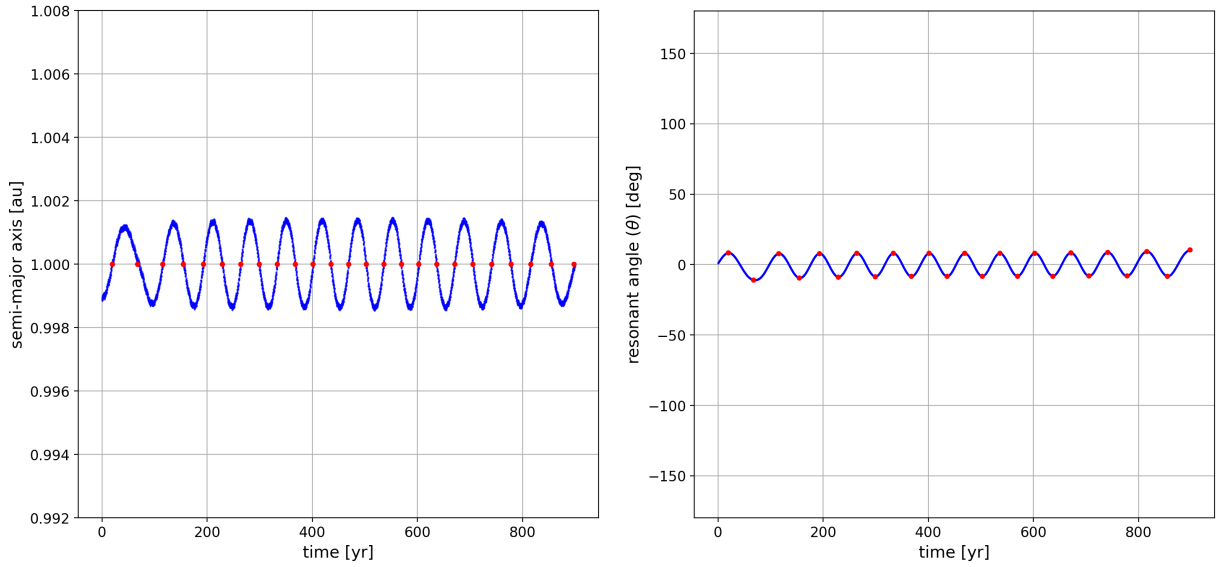


Figure 2: The quasi-satellite behavior of 2004 GU<sub>9</sub> in **(left)** semi-major axis and **(right)** the resonant angle,  $\theta$ . The red points correspond to the  $a = 1$  au crossings. The  $y$ -ranges in both panels of Figs 2-6 are the same to emphasize the differences between them.

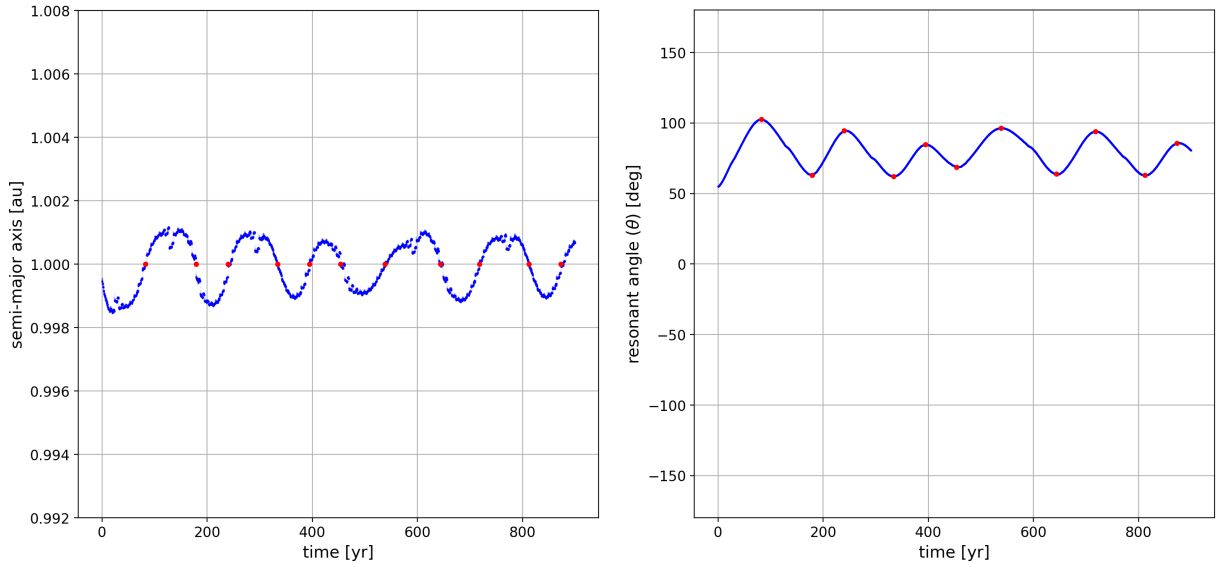


Figure 3: The tadpole behavior of 2020 XL<sub>5</sub> in **(left)** semi-major axis and **(right)** the resonant angle,  $\theta$ . The red points correspond to the  $a = 1$  au crossings.

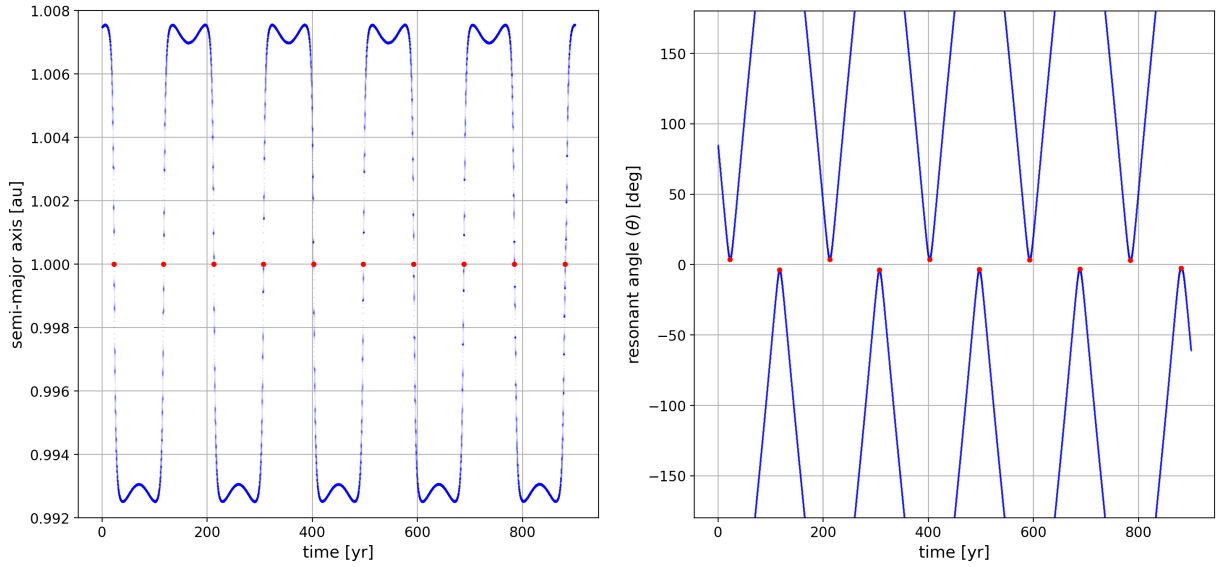


Figure 4: The horseshoe behavior of 2002 AA<sub>29</sub> in **(left)** semi-major axis and **(right)** the resonant angle,  $\theta$ . The red points correspond to the  $a = 1$  au crossings.

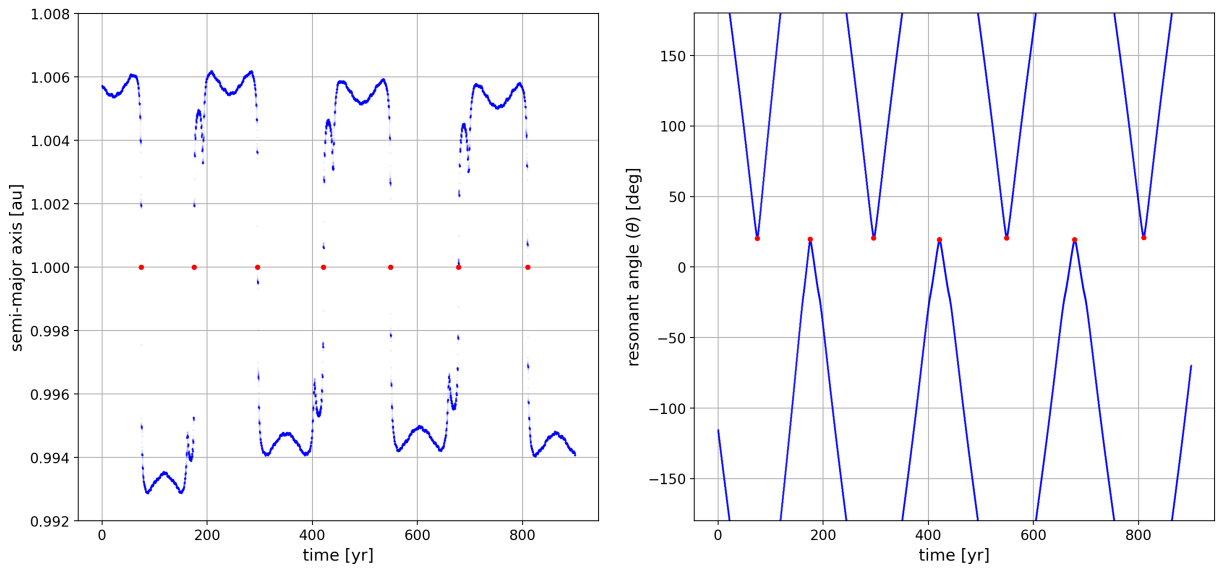


Figure 5: The compound behavior of 2020 CX<sub>1</sub> in **(left)** semi-major axis and **(right)** the resonant angle,  $\theta$ . The red points correspond to the  $a = 1$  au crossings.

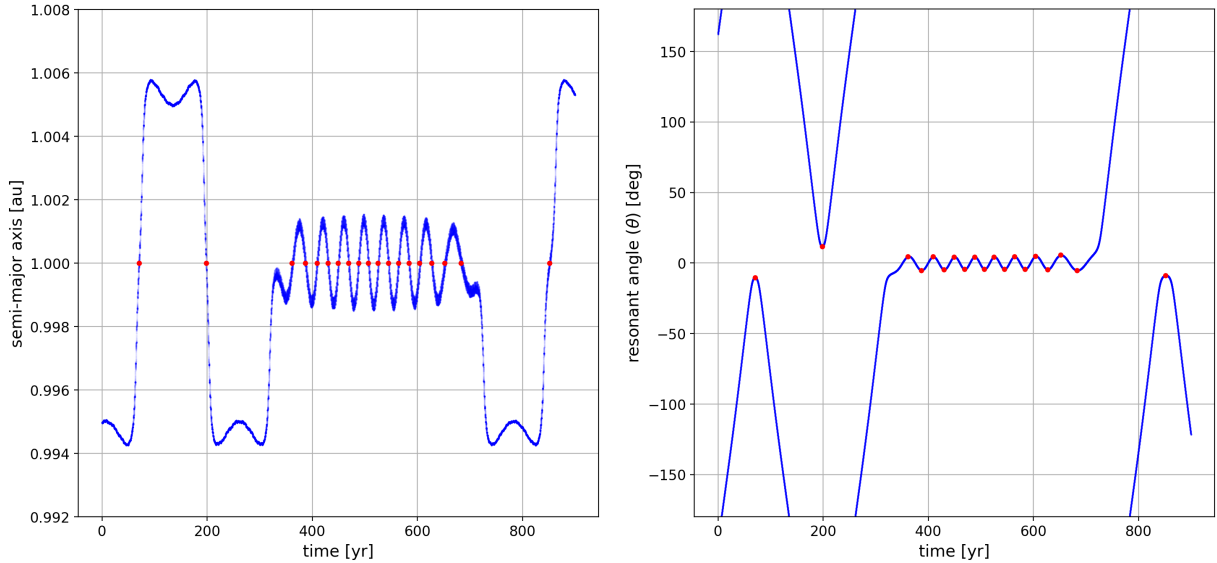


Figure 6: The transition between horseshoe and quasi-satellite motions experienced by (469219) Kamo’oalewa in **(left)** semi-major axis and **(right)** the resonant angle,  $\theta$ . The red points correspond to the  $a = 1$  au crossings.

The algorithm we employed identifies the co-orbital regime by determining the epoch at which  $a = 1$  au (e.g. the red points in the left panels of figs. 2-5) at which the resonant angle is at a local minimum or maximum,  $\theta_{min}$  and  $\theta_{max}$  respectively (e.g. the red points in the right panels of figs. 2-5 where  $d^2\theta/dt^2 > 0$  and  $< 0$  respectively). With this definition it is possible that  $\theta_{max} < \theta_{min}$ . The particles are then associated with a co-orbital regime according to the following criteria:

- *Quasi-satellite (QS)*: when  $(\theta_{max} \times \theta_{min} < 0$  and  $\theta_{max} > \theta_{min})$  or  $(\theta_{max} \times \theta_{min} > 0$  and  $|\theta_{max} + \theta_{min}|/2 < 35^\circ$ , a ‘drifting’ quasi-satellite) ;
- *Tadpole (TP)*: when  $\theta_{max} \times \theta_{min} > 0$  and  $\theta_{max} > \theta_{min}$  and  $|\theta_{max} + \theta_{min}|/2 \geq 35^\circ$ ;
- *Horseshoe (HS)*: when  $\theta_{max} \times \theta_{min} < 0$  and  $\theta_{max} < \theta_{min}$ ;
- *Compound (CP)*: when  $\theta_{max} \times \theta_{min} > 0$  and  $\theta_{max} < \theta_{min}$ .

Known objects in the QS regime (table A.1) experience an  $a = 1$  au crossing (Fig. 2) at least every 20 years, e.g. (469219) Kamo’oalewa, and we required co-orbital interval durations to be  $\geq 100$  yr, i.e. 5 time steps. The behavior of the resonant angle while in a co-orbital regime can be irregular due to  $n$ -body perturbations (figs. 2-6) which is why the conditions on  $\theta$  are more complex than might be expected if we were restricted to the 3-body problem. They also allow for ‘drifting’, secular changes in the average value of the resonant angle, in the quasi-satellite and tadpole regimes, e.g. the middle and right panels of fig. 8, the distinction is that the angle crosses zero for drifting QS, whereas it does not for drifting TP. The value of  $35^\circ$  was selected by examination of the  $(\theta, e)$  map in Pousse and Alessi

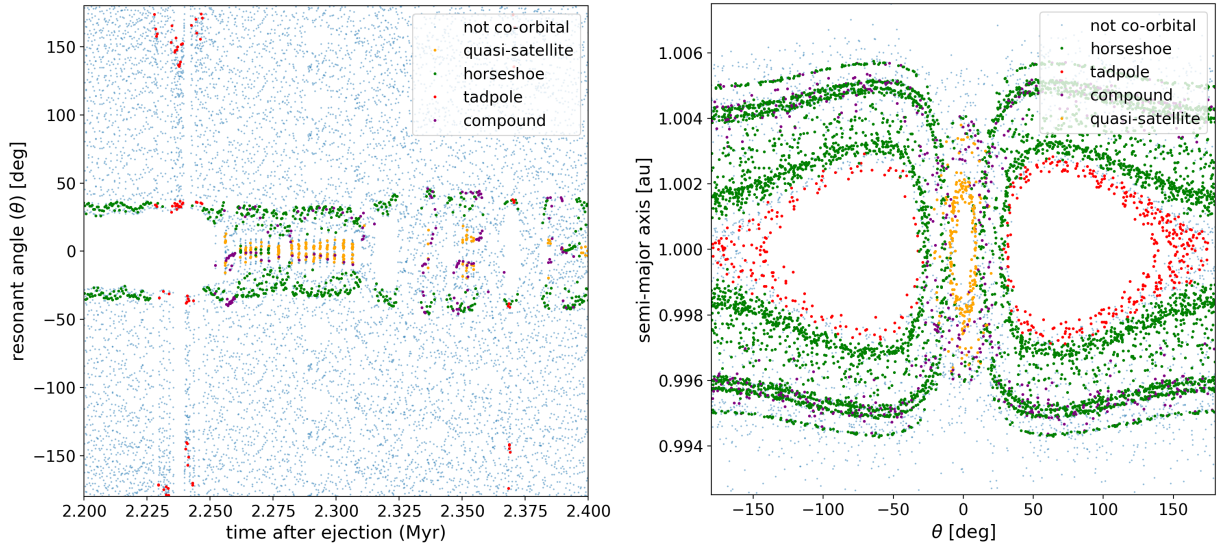


Figure 7: **(left)** The time evolution of the resonant angle,  $\theta$ , over 200 kyr for one of our synthetic lunar ejecta particles indicating times when it is not co-orbital and in a co-orbital regime. **(right)** The behavior of the same particle in  $(\theta, a)$  phase space illustrating well-defined structures corresponding to the different co-orbital regimes. This example corresponds to part of the trajectory shown on the left panel of fig. 1.

(2022) to classify quasi-coplanar co-orbital motion. Moreover, tadpole orbits that stem from  $L_4/L_5$  are not necessarily centered at  $\theta = \pm 60^\circ$  because this value depends on the orbit’s eccentricity (Pousse et al., 2017). Finally, note that particles may exhibit more than one co-orbital behavior in their lifetime and that transitions between regimes may occur with no temporal gap at the resolution of our integrations (fig. 7 and fig. 8).

The co-orbital identification algorithms employed by others are also based on an initial filtering on the semi-major axis followed by a classification of the co-orbital regime based on the oscillation of the resonant angle (e.g. Castro-Cisneros et al., 2023; Jiao et al., 2024; Sfair et al., 2025). Castro-Cisneros et al. (2023) state that their final classification was by visual inspection and their results do not show tadpole behavior while Sfair et al. (2025) implemented an automated methodology.

## 2.2. Co-orbital steady-state populations

Our calculation of the steady-state population of co-orbitals is essentially identical to that developed by Jedicke et al. (2025) for the minimoon population and we refer the reader to that work for the details. It derives from the basic steady-state equation:

$$\bar{n}(d) = \bar{f}(d) \bar{\ell}(d). \quad (2)$$

where  $d$  is an object’s diameter,  $\bar{n}$  is the average number of objects in the steady-state,  $\bar{f}$  is the flux of objects into the population, and  $\bar{\ell}$  is the average lifetime of objects in the steady-state. In this work we use the integrations described briefly above, and in detail in Jedicke et al. (2025), to calculate the average flux and lifetime of objects in co-orbital motion with Earth. The diameter distribution of the co-orbitals is calculated by accounting for the

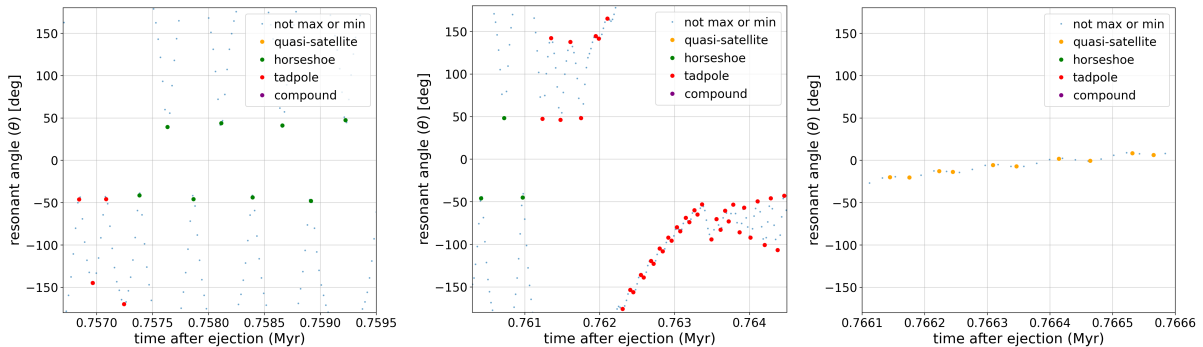


Figure 8: High time resolution behavior of the resonant angle for the synthetic object on the right panel of fig. 1 illustrating transitions between co-orbital regimes and the difference between the QS, TP and HS orbits. **(left)** A transition from the tadpole to horseshoe regimes. **(center)** A transition from the horseshoe to tadpole regime. The particle exhibits a ‘drifting’ resonance angle while in the tadpole regime for times  $\gtrsim 0.7622$  Myr. **(right)** A drifting quasi-satellite regime.

speed, flux, diameter, and density distribution of objects that impact the lunar surface, the diameter of the crater created by the impact, and the size and speed of the material ejected from the crater. The ejecta are then integrated as described in §2.1.

### 3. Results & Discussion

#### 3.1. Known co-orbitals

We applied the procedure described above to the set of known<sup>3</sup> small bodies with  $a \in [0.97 : 1.03]$  au and identified those that exhibit co-orbital behavior in the years 1600-2500 (tables A.1 and A.2, fig. 9). We identified almost 100 objects, most of them in the horseshoe regime or transitioning between co-orbital regimes involving a horseshoe, while 68 are currently co-orbital. The set of objects is not the same as those identified by Di Ruzza et al. (2023) because we have used a different procedure, an updated set of candidates, and have included objects with inclinations  $> 10^\circ$ .

The definition of co-orbital means that all the known objects have semi-major axes of  $\sim 1$  au so it is not surprising that their average semi-major axis is 1.001 au. The objects have a mean eccentricity of  $\bar{e} \sim 0.19$  and mean inclination of  $\bar{i} \sim 7.5^\circ$  but there are a small number of objects with  $e > 0.4$  and  $i > 20^\circ$  which will be discussed below. With a median absolute magnitude of  $H = 26.4$ , corresponding to a diameter<sup>2</sup> of only  $d = 19$  m, these objects are difficult for contemporary asteroid surveys to detect and 76 of them are  $> 10$  m diameter<sup>2</sup> (fig. 10).

<sup>3</sup>Those in NASA’s JPL Small-Body Database at [https://ssd.jpl.nasa.gov/tools/sbdb\\_query.html](https://ssd.jpl.nasa.gov/tools/sbdb_query.html) as of 2025 Nov 19.

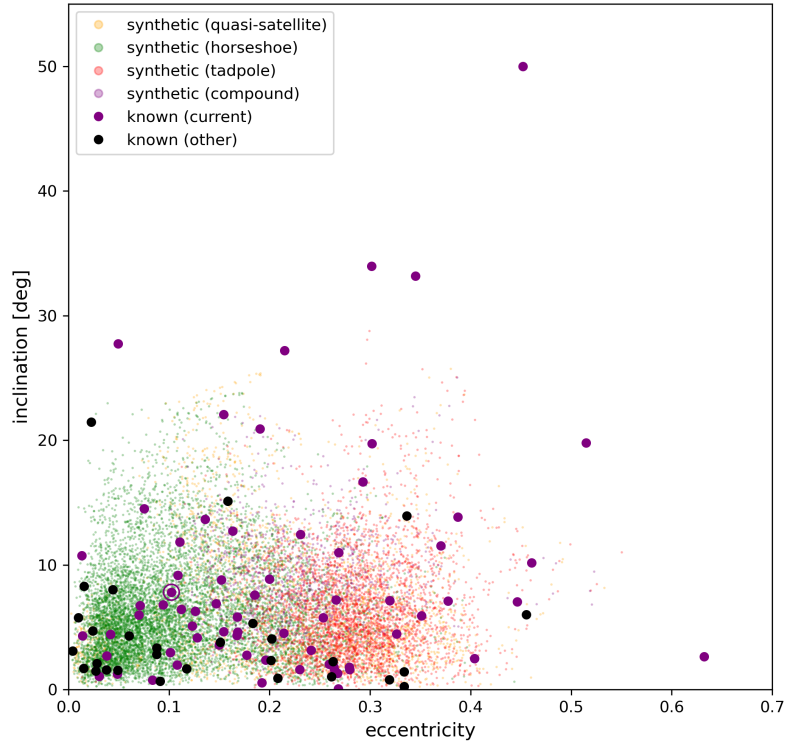


Figure 9: The time-averaged eccentricity and inclination of synthetic Earth co-orbitals that were lunar ejecta over the duration of their time spent in each co-orbital regime. (purple circles) The present-day values of the orbital elements for known asteroids currently in co-orbital motion with Earth (table A.1) and (black circles) known asteroids that were, or will be, co-orbital with Earth in the years 1600-2500 (table A.2). The point representing (469219) Kamo'oailewa is circled.

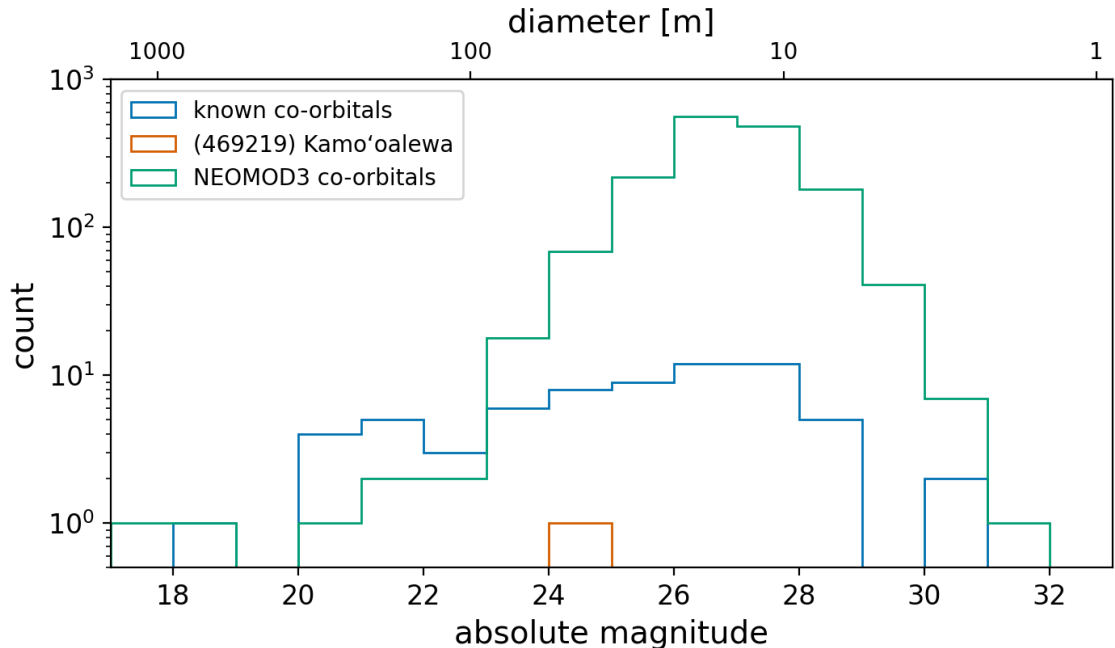


Figure 10: The absolute magnitudes and diameters of Earth’s known co-orbitals and the unbiased synthetic population of co-orbitals generated with NEOMOD3 assuming that the objects have albedos of 0.143 such that  $H = 17.75$  corresponds to a diameter of 1 km.

Table 1: The number of known current co-orbitals, those of 10 m diameter<sup>2</sup>, and those with absolute magnitude  $H < 26$  currently in the specified regime, our nominal prediction for the number of co-orbitals in each regime with a lunar origin, and the total number of co-orbitals expected from the main belt using NEOMOD3 (Nesvorný et al., 2024). The number of objects in the lunar model in any regime is not the sum of the number in the four separate regimes because the regimes have different average durations (i.e., eq. 3). Uncertainties are not included in the nominal lunar model because they are dominated by systematics as discussed in §3.5. The uncertainties on the NEOMOD3 model are simply  $\sqrt{N}$ .

regime	known	known > 10 m	known $H < 26$	nominal lunar	
				model > 10 m	NEOMOD3 > 10 m
any	68	58	37	71	1589±40
quasi-satellite	13	12	6	37	318 ± 18
horseshoe	17	15	9	64	380 ± 19
tadpole	6	6	5	18	783 ± 28
compound	32	25	17	17	108 ± 10

We identified 3 objects in tadpole orbits, 2005 UH<sub>6</sub> ( $L_5$  Trojan), 2005 QQ<sub>87</sub> ( $L_5$  Trojan), and 2024 JR<sub>16</sub> ( $L_4$  Trojan), in addition to the 2 widely known objects, 2010 TK<sub>7</sub> and

Table 2: NEOMOD3-derived main belt source region probabilities for known Earth co-orbitals and the average source region probabilities for the 97 known Earth co-orbitals identified in this work. NEOMOD3 source regions with no values  $> 0.015$  have been omitted. The source regions are the  $\nu_6$  secular resonance, the 3:1, 5:2, and 8:3 mean motion resonances, the inner belt region, and the Hungaria and Phocaea regions.

object	$p_{\nu_6}$	$p_{3:1}$	$p_{5:2}$	$p_{8:3}$	$p_{115}$	$p_{\text{inner}}$	$p_{\text{Hun}}$	$p_{\text{Pho}}$
3753 Cruithne (1986 TO)	0.11	0.32	0.03	0.14	0.06	0.27	0.04	0.01
85770 (1998 UP1)	0.42	0.39	0.01	0.02	0.02	0.08	0.05	0.01
255071 (2005 UH6)	0.35	0.26	0.06	0.02	0.00	0.28	0.04	0.00
706765 (2010 TK7)	0.53	0.20	0.01	0.02	0.00	0.21	0.03	0.00
(2013 LX28)	0.70	0.20	0.00	0.01	0.00	0.04	0.03	0.02
average co-orbital	0.78	0.16	0.00	0.00	0.00	0.05	0.01	0.00

2020 XL<sub>5</sub> (both  $L_4$  Trojans), and verified the synodic behavior of the three objects with the NEOCC visualization tool<sup>4</sup>. 2005 UH<sub>6</sub> has a perihelion distance of 0.37 au and an aphelion distance of 1.63 au so it crosses the orbits of Venus, Earth and Mars, which causes the asteroid’s resonant angle to oscillate around a variable value. With an eccentricity of 0.35, 2024 JR<sub>16</sub> suffers from similar dynamical effects. These two objects were dubbed ‘jumping’ by Pan and Gallardo (2025) and both have orbits with resonant angles that oscillate around a value higher than  $100^\circ$  in absolute value due to their high eccentricities (Pousse et al., 2017). In addition, 2005 QQ<sub>87</sub>’s orbital inclination of  $34^\circ$  contributes to its unusual dynamical evolution (cf. fig. 6f in Christou (2000)).

Assuming that the co-orbitals derive from the main belt per NEOMOD3 (Nesvorný et al., 2024) their orbital elements suggest that they have a 78% probability of being delivered to near-Earth space by the  $\nu_6$  resonance, a 16% chance of being processed through the 3:1 resonance, or a 5% likelihood of a provenance in the forest of minor resonances in the inner region of the belt (table 2). The other nine sources considered by Nesvorný et al. (2024) contribute  $\lesssim 1\%$  each. Given that the 3:1 resonance marks the outer boundary of the inner belt and, for the sake of argument, assuming that half of the objects delivered from that resonance to near-Earth space were originally interior to the resonance, then about 97% of Earth’s known co-orbitals derive from the inner belt. If this is the case then most of these objects should be S-complex objects (e.g. DeMeo and Carry, 2014).

Of the 97 known Earth co-orbitals identified in this work only 5 have *any* NEOMOD3 source probability  $> 1.5\%$  for any source region other than the  $\nu_6$  and 3:1 resonances and the ‘inner’ sources (table 2). Even so, the inner belt remains the most likely source of these 5 objects with the highest non-inner belt source region probability of 14% for 3753 Cruithne (1986 TO) originating in the 8:3 resonance at about 2.71 au. In that region of the belt S- and C-complex asteroids are found in roughly equal proportion (DeMeo and Carry, 2014).

<sup>4</sup><https://neo.ssa.esa.int/orbit-visualiser>

### 3.2. Synthetic main belt co-orbitals

This work was motivated by recent spectroscopic studies of known co-orbitals that suggest they originated on the lunar surface, so it is also important to investigate the number of co-orbitals that can be explained through their dynamical evolution from the main belt. To that end we employed NEOMOD3 (Nesvorný et al., 2024) to generate a pseudo-realistic population of objects that are  $\geq 10$  m diameter with semi-major axes in the range  $0.97 \text{ au} \leq a \leq 1.03 \text{ au}$ . All the objects generated by NEOMOD3 have a main belt or Jupiter family comet (JFC) provenance and the model provided 67,775 objects with no restrictions on eccentricity and inclination. NEOMOD3 does not generate the other three angular orbital elements, the longitude of the ascending node, the argument of perihelion, and the mean anomaly, so we generated each of them in a uniform random distribution in the range  $[0^\circ, 360^\circ)$ .

Using REBOUND we integrated those objects forward and backward by 75,000 days, about 205 yr, in each direction and then identified 1589 of the objects as being co-orbital at the current epoch compared to the 58 known co-orbital objects larger than 10 m diameter<sup>2</sup> (table 1). Taken at face value, and assuming that all the known co-orbitals originated in the main belt or JFC population, it implies that  $\lesssim 4\%$  of the co-orbitals  $> 10$  m diameter have been discovered. On the other hand, NEOMOD3 predicts that there are 6 co-orbital objects  $> 100$  m diameter while there are already 12 known in this size range. We speculate that the excess may be due to errors in NEOMOD3, perhaps due to it not including tidal disruptions of asteroids that pass close to Earth (e.g. Granvik and Walsh, 2024), neglecting a population of objects that originate on the lunar surface, and/or misestimating the observational bias in detecting the smallest asteroids.

The number of co-orbital objects predicted by NEOMOD3 that are similar to (469219) Kamo‘oalewa is of particular interest given that there are claims that it has a lunar-like spectrum (Sharkey et al., 2021; Zhu et al., 2025) and Jiao et al. (2024) specifically link it to the lunar crater Giordano Bruno. We define (469219) Kamo‘oalewa-like objects as co-orbitals with eccentricities within  $\pm 0.05$  and inclinations within  $5^\circ$  of (469219) Kamo‘oalewa’s orbital elements for which there are 44 objects in our NEOMOD3 instantiation. Constraining the similarity specifically to quasi-satellites with  $H < 27$ , (469219) Kamo‘oalewa’s  $H = 24.3$ , suggests that the main belt and JFC sources can generate about 1 (469219) Kamo‘oalewa-like co-orbitals so that invoking a lunar source for this co-orbital is not necessary on dynamical grounds. This is in agreement with Fenucci et al. (2026) who specifically considered the formation of quasi-satellites with a main belt provenance and found that it could produce  $1.23 \pm 0.13$  (469219) Kamo‘oalewa-like objects.

The eccentricity and inclination distributions of the Earth co-orbitals generated with NEOMOD3 cover the entire range of values of the known co-orbitals (fig. 11) suggesting that the main belt and JFC are viable source regions for these objects. The average eccentricity and inclination of the NEOMOD3 co-orbitals are 0.28 and  $15.9^\circ$  respectively. About 50% of the NEOMOD3 co-orbitals are on tadpole orbits in contrast with the  $\sim 14\%$  of known objects with  $H < 26$ . These tadpoles have oscillation periods in their resonant angles of about 400 years and the resonant angle is shifted towards  $\pm 100^\circ$ , like 2005 UH<sub>6</sub>, 2005 QQ<sub>87</sub>, and 2024 JR<sub>16</sub> (table 3 and table A.2). This is likely an observational selection effect since

Table 3: Selected properties of known Earth co-orbitals with  $e > 0.5$  and  $i > 25^\circ$  which are likely to have a main belt provenance in order of discovery year. The absolute magnitude,  $H$ , is from JPL Horizons<sup>b</sup> and the diameter is calculated from  $H$  assuming that all objects have an albedo of 0.143 which maps  $H = 17.75$  to a diameter of 1000 m. Taxonomic classes and citations are from ESA’s near-Earth objects coordination centre.<sup>c</sup> We provide one reference to other works that mention these objects.

number	name	designation	H	diameter [m]	taxonomic class <sup>a</sup>	references [e.g.]
3753	Cruithne	1986 TO	15.4	2924	Q	<a href="#">Wiegert et al. (1997)</a>
85770		1998 UP <sub>1</sub>	20.7	255	S	<a href="#">Galiazzo and Schwarz (2014)</a>
255071		2005 UH <sub>6</sub>	18.4	755	n/a	<a href="#">Birlan et al. (2010)</a>
		2005 QQ <sub>87</sub>	22.8	96	n/a	<a href="#">Tardioli et al. (2017)</a>
		2013 LX <sub>28</sub>	21.9	149	n/a	<a href="#">Connors (2014)</a>
		2016 CA <sub>138</sub>	23.3	77	n/a	<a href="#">Borisov et al. (2023)</a>
		2017 XQ <sub>60</sub>	24.5	45	n/a	<a href="#">Kaplan and Cengiz (2020)</a>

<sup>a</sup>[DeMeo et al. \(2014\)](#), <sup>b</sup><https://ssd.jpl.nasa.gov/horizons>,

<sup>c</sup><https://neo.ssa.esa.int/search-for-asteroids>

the minimum resonant angle for a tadpole is  $25^\circ$  so the minimum distance between Earth and an object is  $\sim 0.43$  au when it is only  $77.5^\circ$  from the Sun, an area that is difficult for asteroid surveys to image. Furthermore, an  $H = 26$  object has an apparent magnitude of  $V \sim 26.9$ , about 5 magnitudes fainter than the Pan-STARRS limiting magnitude, the most sensitive dedicated, long-term asteroid survey to-date ([Denneau et al., 2013](#)). An object would need to have an absolute magnitude of  $H \lesssim 21$  to be brighter than the Pan-STARRS limiting magnitude even when surveying in the bright sky in the direction of morning or evening twilight. Co-orbital objects in the other 3 regimes can experience periods when their resonant angle is near zero which brings them closest to Earth during which time they are more likely to be discovered. Thus, we predict that there is a large population of undetected tadpole co-orbitals and that the Vera Rubin Observatory will detect many during its twilight survey campaign (e.g. [Schwamb et al., 2023](#); [Bolin et al., 2025b](#)), in agreement with the prospects for discovery of lunar ejecta calculated by [Wu et al. \(2026\)](#).

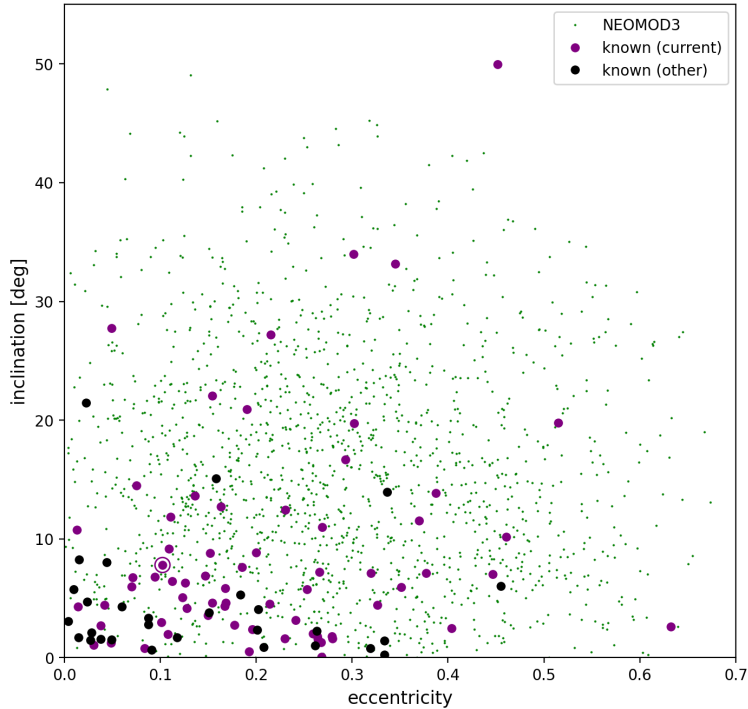


Figure 11: The eccentricity and inclination of synthetic Earth co-orbitals that have a main belt or JFC provenance according to NEOMOD3. (purple circles) The present-day values of the orbital elements for known asteroids currently in co-orbital motion with Earth (table A.1) and (black circles) known asteroids that were, or will be, co-orbital with Earth in the years 1600-2500 (table A.2). The point representing (469219) Kamo’oalewa is circled.

### 3.3. Synthetic lunar co-orbitals

We then applied the procedure for identifying periods of co-orbital motion to our synthetic population of lunar ejecta while in heliocentric orbit.

The eccentricity and inclination distributions of the lunar ejecta co-orbitals (fig. 9) are different from the Earth co-orbitals in NEOMOD3 (fig. 11) — they are more concentrated at low- $e$  and low- $i$  than the main belt/JFC co-orbital population. The maximum eccentricity is 0.55 and the maximum inclination is  $29^\circ$ , i.e. all the lunar ejecta co-orbitals are on heliocentric prograde orbits. This could be an artifact of the method described in Jedicke et al. (2025) that removes objects that ‘leave the ‘extended intermediate source region’ (xISR) defined by heliocentric semi-major axes in the range  $a \in [0.8 \text{ au}, 1.2 \text{ au}]$ , eccentricities in the range  $e \in [0, 0.2]$ , and inclinations in the range  $i \in [0^\circ, 5^\circ]$ ’ but we think it is unlikely that an object’s orbital elements can evolve outside the xISR and then evolve onto a retrograde orbit with  $a \sim 1$ . While retrograde orbits exist in the circular restricted three-body problem (Morais and Namouni, 2013b) and have been identified in association with Jupiter and Saturn (Morais and Namouni, 2013a; Wiegert et al., 2017) none exist amongst Earth’s known co-orbitals.

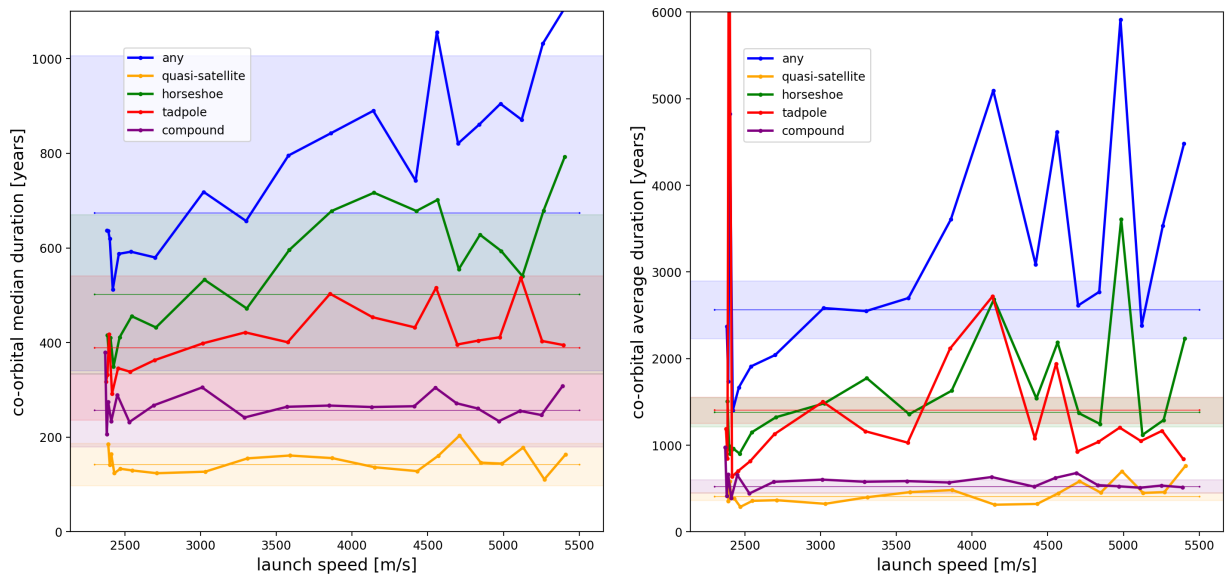


Figure 12: **(left)** The points connected by solid piecewise lines represent the median duration of co-orbital motion in each of the four regimes and any regime as a function of launch speed from the lunar surface. The data points are offset by  $(0, \pm 5, \pm 10) \text{ m s}^{-1}$  from their actual values to improve readability. The uncertainty on the duration at each launch speed for each regime is not shown for clarity. Thin solid horizontal lines represent the weighted mean duration of the median values for the regime while the shaded bands represent the standard error on the means. **(right)** Similar to the left panel except for the average duration of co-orbital motion instead of the median. Note the different scales on the  $y$ -axis.

Table 4: The average eccentricity and inclination and RMS of the distributions for synthetic lunar ejecta for each of the Earth co-orbital classes. The uncertainties are the standard error on the mean. The values correspond to all the particles in our integrations that became co-orbital; they are not weighted by the number of co-orbitals generated at each speed.

class	eccentricity		inclination [deg]	
	mean $\pm\sigma$	RMS	mean $\pm\sigma$	RMS
quasi-satellite	0.215 $\pm$ 0.002	0.24	6.94 $\pm$ 0.10	8.6
horseshoe	0.111 $\pm$ 0.001	0.13	6.24 $\pm$ 0.04	7.4
tadpole	0.284 $\pm$ 0.001	0.29	6.41 $\pm$ 0.07	7.5
compound	0.228 $\pm$ 0.002	0.24	9.28 $\pm$ 0.12	10.0

In the quasi-coplanar approximation each co-orbital regime is associated with a different range in eccentricity and resonant angle (e.g. [Pousse and Alessi, 2022](#); [Cortese et al., 2025](#)) and, assuming that the  $(e, \theta)$  phase-space is uniformly populated, we would expect that the tadpoles would be the most populous with a mean  $e < 0.5$ , the QS would be the next most likely regime with  $e > 0.5$ , and the HS co-orbitals would be the least populated. These expectations are modified by the initial conditions of the synthetic lunar ejecta which preferentially generate co-orbitals with low eccentricity. Furthermore, particles with  $e > 0.5$  are likely to have close encounters with Venus and Mars so they will be short-lived and not contribute much to the population statistics. Thus, our results differ from our naive expectations. There are statistically significant differences between the mean eccentricities of the synthetic lunar co-orbitals in the different regimes with the horseshoe co-orbitals having the lowest  $e$  while the tadpoles have a value about  $2.5\times$  larger (table 4). There are also statistically significant differences in the mean inclinations of the co-orbital particles but the compound regime’s inclination is  $\gtrsim 15\sigma$  from the other three regimes because they can only exist in the inclined case.

The *biased*  $(e, i)$  distribution of known objects that undergo co-orbital episodes between years 1600 and 2500 (table A.1 and table A.2) closely matches the corresponding distribution for the synthetic lunar ejecta. This agreement suggests that a lunar origin for at least some known Earth co-orbitals is plausible (fig. 9). Seven objects are notable outliers from this match and are more consistent with a main-belt origin (table 3). It is no surprise that the largest of the seven, the first identified Earth co-orbital, (3753) Cruithne ([Wiegert et al., 1997](#)), was discovered 12 years earlier than the second object, and that the absolute magnitudes of the objects increase with discovery year because they are more difficult to detect and required the advent of superior asteroid surveys. Its size alone would suggest that it is unlikely to be lunar ejecta and it is consistent with being the largest of the co-orbitals with a main belt provenance (table 10). Only the first two discovered objects have taxonomic classifications and both are consistent with a main belt origin. The Q-class (3753) Cruithne is indicative of a fresh surface on an ordinary chondrite-like body while the S-class 1998 UP<sub>1</sub> is the more weathered version (e.g. [Jedicke et al., 2004](#); [Binzel et al., 2010](#)) of the same type

of object, so that both objects can be associated with a main belt origin. Furthermore, it has been suggested that 1998 UP<sub>1</sub> is likely to have been a Hungaria asteroid, a population of objects found on the inner edge of the main belt (Galiazzo and Schwarz, 2014). While the other objects have not been assigned taxonomies the ‘[r]ecoverly prospects for [2013 LX<sub>28</sub>] are excellent’ (Connors, 2014), so we expect that this object and others will be utilized to test the provenance of Earth’s co-orbitals.

We note that four of the co-orbitals in table 3, objects that are more likely of main belt origin according to our analysis, also appear in the table of five co-orbitals with possible origins beyond the inner main belt according to NEOMOD3 (table 2). The co-orbital 1998 UP<sub>1</sub> is the most likely of the five to originate in the Hungaria population with a 5% probability which provides some support for Galiazzo and Schwarz (2014)’s hypothesis.

The duration of co-orbital motion of the particles in our simulation ranged from tens of years to a Myr but the most likely durations were in the hundreds to few thousand year range. The median durations in each regime are well behaved as a function of launch speed and are either flat or increase with launch speed (fig. 12 left). We provide the median durations to illustrate that the behavior of the durations are more regular than suggested by the average durations which are necessary for calculating the steady-state population (eq. 2 and §3.4). The average durations of co-orbital motion are about a few times larger than the median durations but with high RMS due to the statistics of a small number of long duration events (fig. 12 right). Note that the average duration of ‘any’ co-orbital,  $\mu_{any}$ , is not the sum of the averages of the individual regimes but is given by

$$\mu_{any} = \frac{1}{n_{any}} (n_{QS}\mu_{QS} + n_{HS}\mu_{HS} + n_{TP}\mu_{TP} + n_{CP}\mu_{CP}), \quad (3)$$

where  $n_{any}$  is the number of continuous co-orbital intervals, i.e. such that the transitions from one regime to another are not interrupted by non-resonant intervals,  $n_X$  is the number of intervals corresponding to regime  $X$ , and  $\mu_X$  denotes the average duration in the regime.

We fit the average durations as a function of launch speed to straight lines and found that two of the four regimes are consistent with being constant and the other two were within  $3\sigma$  of being flat. Particles in ‘any’ regime also exhibit  $< 3\sigma$  deviation from a linear trend with launch speed. Given that the median durations are well behaved, the average durations are consistent with being constant within  $3\sigma$ , and we will show below that the systematic uncertainties in the lunar ejecta size-frequency distribution overwhelm our assumptions on the relationship between co-orbital duration and launch speed. We used the weighted mean over all launch speeds within a regime as the canonical duration time for objects regardless of their launch speed. We will employ the standard error on the mean for our systematic study of the uncertainties on the steady-state size-frequency distribution in §3.5.

The thousand to a few 1,000 years average durations for our lunar co-orbitals is dramatically shorter than the 25,000 year lifetime of co-orbitals of main belt origin calculated by Morais and Morbidelli (2002). While they predicted that there are  $0.65 \pm 0.12$   $H < 18$  Earth co-orbitals and  $16.3 \pm 3.0$  with  $H < 22$ , in good agreement with the 1 and 11 currently known respectively, we note that their source population is different from ours, aligned with the results in §3.3 and, more importantly, their output time was 100 years and they rejected

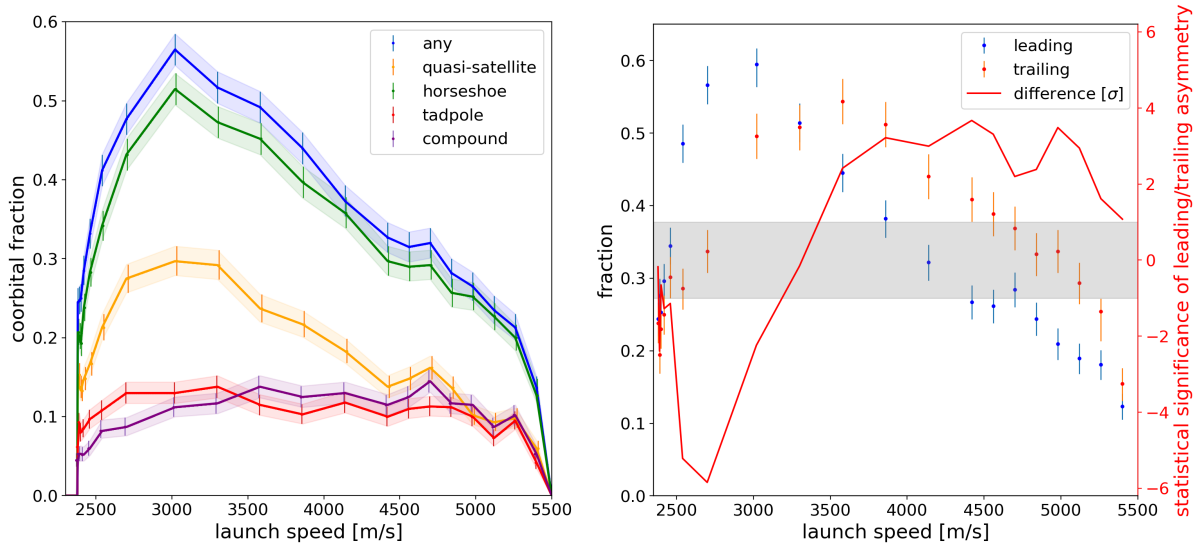


Figure 13: (**left**) The average fraction of particles that experience different, or any, regimes of co-orbital motion as a function of their lunar ejection speed. The solid lines are a piecewise-continuous linear function that connect the data points. The coloured bands are the  $\pm 1$ -sigma regions that are used in our study of the systematic uncertainty on the co-orbitals’s steady-state size-frequency distribution. The functions representing the average fractions are forced to zero for launch speeds  $< 2380 \text{ m s}^{-1}$  and for speeds  $\geq 5500 \text{ m s}^{-1}$ . (**right**) The fraction of particles that experience at least one co-orbital period as a function their launch speed for particles ejected from leading ( $< 0$ ) or trailing lunar longitudes ( $\geq 0$ ). The right hand  $y$ -axis provides the statistical significance of the difference between the leading/trailing asymmetry.

cases shorter than 1,000 years. This would have the effect of lengthening the average duration of their co-orbitals. They also noted that “the typical eccentricities are quite high, that most objects have orbits which are Venus crossing ( $e > 0.28$ ), and that many have orbits which are Mars crossing ( $e > 0.52$ ). ... typical inclinations can also be quite high and that most of the objects have orbits with  $10^\circ < i < 45^\circ$ ”, in line with our analysis of co-orbitals with a main belt provenance in §3.2.

We attributed that fact that the durations are independent of launch speed to the particles ‘forgetting’ their launch conditions in the time between ejection and the co-orbital period. We then investigated whether the co-orbitals had a ‘memory’ of their ejection speed revealed in their eccentricity distributions. We found that the quasi-satellite, tadpole, and compound co-orbitals do not show significant correlations between launch speed,  $v$ , and their eccentricity during their co-orbital periods but the horseshoe co-orbitals do, with  $\bar{e} = (0.0114 \pm 0.0008)v + (0.065 \pm 0.003)$ . We found an even stronger correlation between the mean eccentricity of  $e < 0.1$  QS co-orbitals<sup>5</sup> and their launch speeds of  $\bar{e} = (0.017 \pm 0.001)v + (-0.018 \pm 0.003)$ . While the range of eccentricities is large at any launch speed these results suggest that high- $e$  HS co-orbitals are more likely to have been ejected at high speed and it would therefore be unusual to discover a large, high- $e$  HS co-orbital.

<sup>5</sup>There is a gap in the quasi-satellites’ eccentricity distribution at  $e \sim 0.1$  that we leave for examination to future work.

All the launch speeds we considered can generate co-orbitals and the fraction of particles that become co-orbital exceeds 50% for launch speeds  $\gtrsim 2800 \text{ m s}^{-1}$  and  $\lesssim 3500 \text{ m s}^{-1}$  (fig. 13). The maximum fraction of  $\sim 57\%$  occurs at a launch speed of  $3020 \text{ m s}^{-1}$ , the same value which maximizes the fraction of ejecta that become ‘temporarily bound objects’, with a negative total energy with respect to the geocenter (Jedicke et al., 2025). Sfair et al. (2025) identified a peak in co-orbital production associated with an ejection speed of  $2880 \text{ m s}^{-1}$ . While the horseshoe and quasi-satellite co-orbital regimes follow the same trend as objects in any co-orbital regime, the compound and tadpole co-orbitals display a different behaviour with a broad maximum fraction extending from about  $2750 \text{ m s}^{-1}$  to over  $5000 \text{ m s}^{-1}$ . Castro-Cisneros et al. (2023) found that only 6.6% of their ejecta achieved co-orbital motion and those most likely to achieve co-orbital status were launched at ‘slightly above lunar escape’ speed where our work suggests that the launch speed most likely to result in co-orbital motion is about  $600 \text{ m s}^{-1}$  greater than the escape speed.

We found that there is a launch speed dependent asymmetry in the fraction of test particles that become co-orbital from the Moon’s leading and trailing hemispheres (fig. 13, right) in contrast with Castro-Cisneros et al. (2023) who found that the trailing side generated more co-orbitals. The actual asymmetry in the overall fraction of lunar ejecta that become co-orbital is then also a function of the number of particles ejected as a function of launch speed. The statistical significance of the asymmetry at each launch speed is  $> 1\sigma$  at most of the speeds we examined and  $> 3\sigma$  over a wide range of launch speeds.

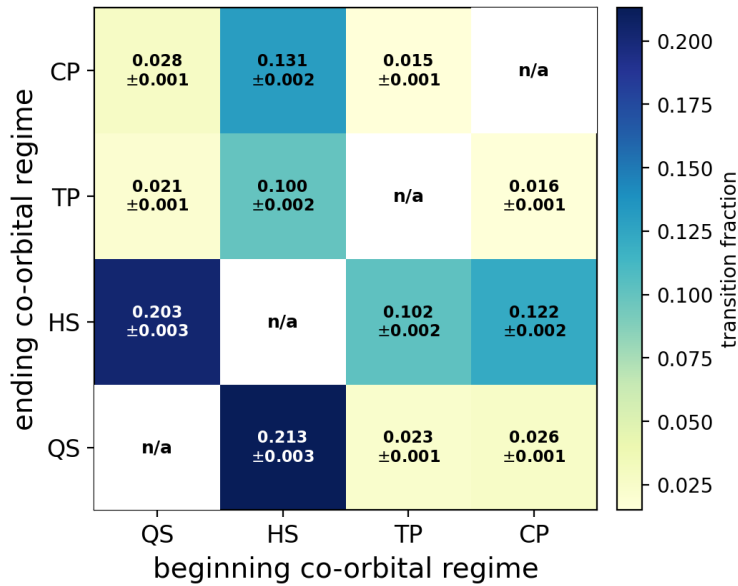


Figure 14: The fraction of all co-orbital transitions that are from the beginning to ending regime.

Transitions between co-orbital regimes, i.e. where a particle makes a transition without a non-resonant period between the regimes, have been studied for specific transitions and objects (e.g. Christou, 2000; Brassler et al., 2004; Wajer, 2010) but we investigated the transition probabilities between all four regimes. The computed fractions are generally consistent

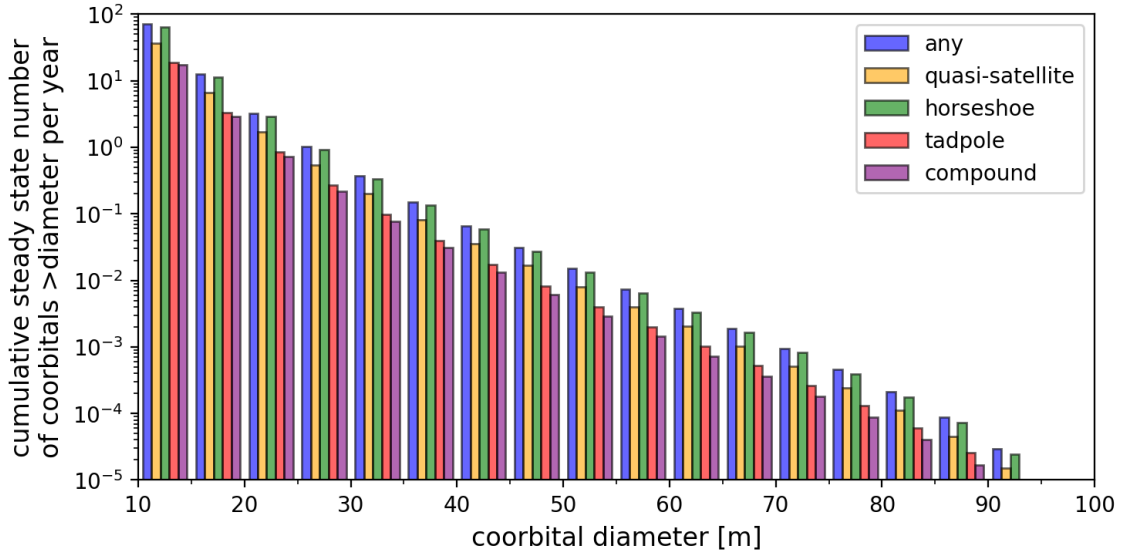


Figure 15: The nominal cumulative steady-state SFD of Earth’s co-orbitals that originate as lunar ejecta as a function of diameter and their co-orbital regime in bins of 5 m width.

with those already identified in the Sun-Earth system (e.g. [Brasser et al., 2004](#); [Wajer, 2010](#)). We found that they are mostly symmetric with the most statistically significant asymmetry of  $\sim 2.8\sigma$  between the QS $\rightarrow$ HS and HS $\rightarrow$ QS transitions (fig. 14). Transitions between those two regimes are also the most likely, comprising  $\gtrsim 20\%$  of all jumps between co-orbital states, the most studied and identified, and the one exhibited by (469219) Kamo’oalewa. The relatively high probability of HS $\leftrightarrow$ CP transitions is expected as they have the same nature as HS $\leftrightarrow$ QS transitions, the difference being that CP co-orbitals experience half the resonant angle range of QS co-orbitals. We also expected QS $\leftrightarrow$ TP transitions to be difficult because they can occur at non-negligible inclinations. It would be interesting to analyze these transitions in detail: as a function of inclination, and with respect to eccentricity to determine if they are associated with close approaches to Venus or Mars, and also to the behavior in the argument of pericenter ([Namouni, 1999](#)).

### 3.4. Co-orbital steady-state populations

Our nominal prediction is that there are 71 Earth co-orbitals larger than 10 m diameter in the steady-state population that originated on the Moon’s surface (fig. 15 and table 1) using the central values for the flux, diameter, and density distribution of objects that impact the lunar surface, the diameter of the crater created by the impact, and the size and speed of the material ejected from the crater (following [Jedicke et al. \(2025\)](#)). There is an orders-of-magnitude systematic uncertainty on the number, as was found for the population of ‘temporarily bound objects’ with a negative total energy with respect to the geocenter ([Jedicke et al., 2025](#)), that is addressed in the following sub-section. Most of the remaining discussion focuses on the nominal result with the caveat that the systematic uncertainty is large.

The lunar ejecta co-orbital population is primarily composed of objects in the horseshoe regime followed by quasi-satellites, tadpoles and compound objects (table 1). The number of known co-orbital objects in each regime is within a factor of a few of the predicted number of objects with a lunar provenance, and the total number of objects in any co-orbital regime matches the lunar origin prediction to better than 5%, but this agreement must be spurious because the known population is biased by observational selection effects while the nominal lunar prediction is for the entire population of co-orbitals.

Taken at face value, our nominal lunar provenance model for Earth’s co-orbitals predicts that the Moon provides roughly  $1/23$  ( $\sim 0.043$ ) of the steady-state population relative to the main belt. Our prediction for the number of quasi-satellites  $> 50$  m diameter, the size range corresponding to (469219) Kamo’oalewa, is 0.008 (fig. 15). Fenucci et al. (2026) calculated that the number of (469219) Kamo’oalewa-like quasi-satellites produced specifically by the impact that generated the Giordano Bruno crater would be about 0.042, a factor of  $\sim 5$  greater than our value. While the two calculation methods are not identical we think that they can be compared to one another. Our value corresponds to the steady-state number due to the formation of craters averaged over a long period of time while their value is for the recent, 1-10 Myr ago formation of the large, and therefore rare, Giordano Bruno crater (e.g. Morota et al., 2009). Our formulation suggests that launching a (469219) Kamo’oalewa-like object of 50 m diameter requires an  $\sim 10$  km-scale impactor with an impact frequency of only about 1 per more than 20,000 Myr at the current time. Thus, our results suggest that (469219) Kamo’oalewa is unlikely to have been ejected by the impactor that formed the Giordano Bruno crater but, if it did so recently, then we expect that the number of (469219) Kamo’oalewa-like objects in the current population would be  $> 0.008$  as predicted by Fenucci et al. (2026).

Scaling our results for the predicted population of quasi-satellites of main belt provenance from our NEOMOD3 result<sup>6</sup> we predict that there should be  $\sim 42$  quasi-satellites at the current time with  $H < 26$  and a main belt provenance, only about 40% larger than the 30 suggested by Fenucci et al. (2026). The difference is likely due to our use of less restrictive ranges in  $(a, e, i)$  when selecting candidate co-orbitals and our definitions of the co-orbital regimes. Restricting our identified NEOMOD3 co-orbitals to  $e < 0.2$  and  $i < 20^\circ$  per Fenucci et al. (2026) reduces our predicted co-orbital QS population of main belt provenance to 15.

Fenucci et al. (2026) simulated the discovery efficiency of asteroid surveys up to 2022 and found that they would have discovered about 14% of the quasi-satellites with  $H < 26$ . The quasi-satellite discovery efficiency would increase slowly with time because they have long synodic periods so we would expect there to be about 6 known quasi-satellites with  $H < 26$  ( $\gtrsim 20$  m diameter<sup>2</sup>) in excellent agreement with the 6 we identified in the known population (table 1, and the 3 identified by Fenucci et al. (2026)). Once again, the differences in the predicted numbers are likely a consequence of the range of orbital elements for candidate co-orbitals and the co-orbital regime definitions. We think that the agreement is good given the differences and both results suggest that a lunar source is not necessary to explain

---

<sup>6</sup>From table 1 we have 318 quasi-satellites and we use the canonical Dohnanyi (1969) SFD of  $\log N \propto H/2$  to scale from the 10 m population ( $H = 27.75$ ) to  $H = 26$  ( $\sim 35$  m diameter<sup>2</sup>).

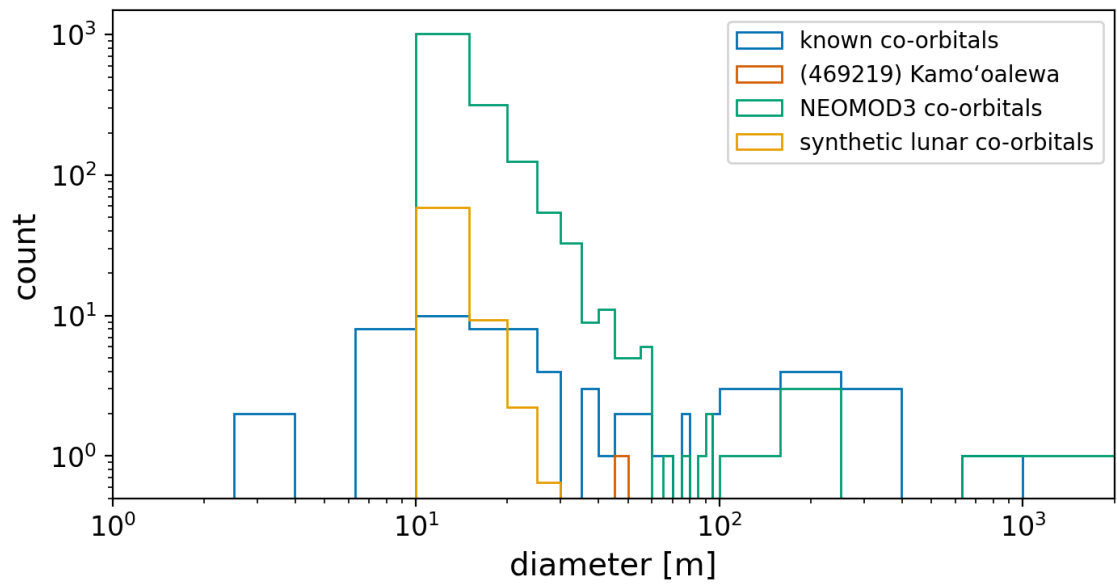


Figure 16: The incremental diameter distributions of the known Earth co-orbitals<sup>2</sup> with (469219) Kamo'oalewa highlighted, the population of synthetic co-orbitals of main belt provenance suggested by NEOMOD3 (Nesvorný et al., 2024), and the nominal distribution of co-orbitals with a lunar origin as calculated in this work. We have attempted to highlight the diameter range where we have calculated the lunar Earth co-orbital SFD by gerrymandering the bins so there are 5 equal-size logarithmic bins in the range from 1-10 m, 20 bins of 5 m width in the 10-100 m range, and 6 equal-size logarithmic bins in the range from 100-2000 m.

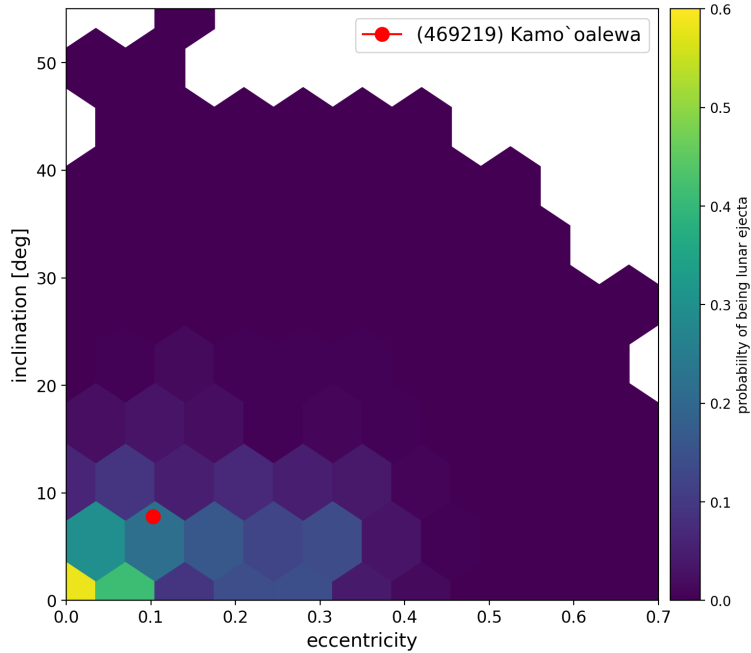


Figure 17: The probability that an Earth co-orbital is lunar ejecta versus originating in the main belt or JFC regions assuming our nominal lunar ejecta co-orbital SFD and the NEOMOD3 population (§3.2) as a function of eccentricity and inclination. White hexes are presumably  $\sim 0$  but we do not have synthetic objects of either provenance in those bins. The red dot represents (469219) Kamo'oalewa's orbital elements but note that the probability, like our ejecta simulations, does not account for an object's mass/size.

the co-orbital population statistics even though some of their colors and spectra suggest otherwise.

Figure 16 highlights how (469219) Kamo'oalewa is unusually large for a co-orbital of lunar origin given our nominal simulations but not unexpected for co-orbitals with a main belt provenance. It is no surprise that the synthetic populations of main belt and lunar material have similar size-frequency distributions because both populations are fragments produced in powerful collisions between objects of comparable densities and material strengths. The known co-orbital population is strongly biased by observational selection effects, such that the population is skewed towards large objects and severely incomplete for objects in the decameter size range.

Jedicke et al. (2025) suggested that the population of minimoons or, more generally, objects temporarily bound to Earth, could be used to constrain parameters that determine the size-frequency distribution of objects that originated on the Moon. The SFD of these objects is particularly sensitive to the crater scaling relation, the crater ejecta size distribution, and the relationship between ejecta mass and speed, so that determining whether they are of lunar origin and then measuring their SFD could shed light on all those processes.

In the same way, the SFD of lunar co-orbitals in the regimes studied in this work would be even more useful given that they are larger, more common, and remain visible for longer durations.

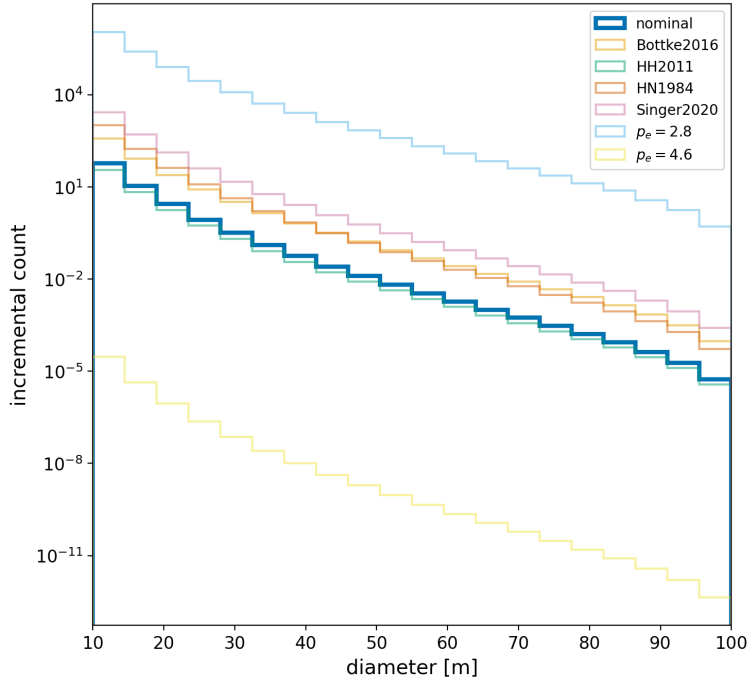


Figure 18: Our nominal steady-state SFD of Earth co-orbitals with a lunar provenance and the SFD using four other crater-scaling relations and  $\pm 1\sigma$  values on the ejecta’s SFD where the number of ejecta with diameters larger than  $d$  is  $N(> d) \propto d^{-p_e}$ . The nominal scaling relation is from Collins et al. (2005), Bottke2016 = Bottke et al. (2016), HH2011 = Housen and Holsapple (2011), HN1984 = Horedt and Neukum (1984) Singer2020 = Singer et al. (2020). The nominal value of  $p_e = 3.7$  was used in Jedicke et al. (2025) which was an average of values from Bart and Melosh (2010).

The probability that a co-orbital is of lunar provenance ( $p_{lunar}$ , fig. 17) is a function of eccentricity and inclination

$$p_{lunar}(e, i) = \frac{n_{lunar}(e, i)}{n_{lunar}(e, i) + n_{MB}(e, i)} \quad (4)$$

where  $n_{lunar}$  and  $n_{MB}$  are number of co-orbitals of lunar and main belt origin using our nominal lunar and NEOMOD3 results respectively. The maximum probability is about 58% for  $e \sim 0$  and  $i \sim 0^\circ$ , decreasing to effectively 0% for  $e \gtrsim 0.45$  or  $i \gtrsim 25^\circ$ . These probabilities should be viewed with suspicion because of the tremendous systematic uncertainties in the lunar co-orbital population (§3.5) but the trend will not be affected. Thus, our results predict that if there are co-orbitals of lunar origin they are significantly more likely to be objects

with low eccentricity and inclination. The nominal probability that (469219) Kamo‘oalewa is of lunar origin is 21% based only on its orbital elements, not accounting for its size as discussed above.

The disagreement between our nominal prediction for the population of co-orbitals with a lunar origin and the spectroscopic evidence that some of these objects have surfaces consistent with the lunar surface suggests that there are errors in our assumptions and/or the values we employed in e.g., the crater scaling relations or the ejecta’s size-speed relationship. Alternatively, the association of co-orbital spectra with lunar material may be called into question as even (469219) Kamo‘oalewa has been spectroscopically connected with the inner main belt Flora family (Zhang et al., 2024). Thus, we encourage more characterization of Earth’s co-orbitals to clarify the provenance of these objects.

### 3.5. Systematic uncertainties

Jedicke et al. (2025) performed a systematic analysis of most of the important parameters employed in their calculation of the steady-state SFD of temporarily bound objects with a lunar provenance and found that there were many orders of magnitudes systematic uncertainty in their model. Given that this analysis implements the same methodology but applied to Earth’s co-orbitals, there are also many orders of magnitude uncertainty in our nominal results (fig. 18). Rather than re-perform their study we provide a few examples of the impact of a few of the important input parameters on our results.

The SFD of the lunar ejecta in the cratering event induces  $\pm 5$  orders of magnitude range in the predicted number of Earth co-orbitals  $> 10$  m diameter of lunar origin extending from  $\sim 10^{-5}$  to  $> 10^5$  (fig. 18). The choice of crater-scaling relation, the functional form of the relationship between an impactor’s properties and the final diameter of the crater, changes the predicted number of ejecta by 2 orders of magnitude while our nominal prediction lies on the lower end of co-orbital SFDs produced by five relations.

The most surprising aspect is that our nominal prediction produces values that are not outrageously out-of-order with the observed population and this suggests that the formal uncertainties on the input parameters may be over-estimated. It also suggests that determining the SFD of co-orbitals with a lunar spectra could assist the effort to constrain our understanding of the crater formation process including crater-scaling relations, the SFD of lunar ejecta, and their size-speed relationship.

## 4. Conclusions

We have calculated the steady-state number of Earth co-orbitals ejected by impacts on the lunar surface by asteroids and comets, performed an independent determination of the number of known co-orbitals, and estimated the number of co-orbitals expected from the main belt utilizing a realization of the population of near-Earth objects with a main belt and cometary provenance.

The algorithm used to classify co-orbital motion allows for the detection of co-orbital transitions. The relative fraction of transitions between the four co-orbital regimes matches our expectations with QS $\leftrightarrow$ HS transitions being the most common and QS $\leftrightarrow$ TP being

uncommon. The computed fractions are consistent with the ones observed so far in the Sun-Earth system.

Our calculation of the expected number of co-orbitals that originated as lunar ejecta has approximately  $\pm 5$  orders of magnitude systematic uncertainty due to uncertainties on the model’s input parameters such as the crater-scaling relation, the size-frequency distribution of the ejecta liberated by the impact, and the size-speed relationship of the ejecta. Ignoring both the statistical and systematic uncertainties, our nominal prediction is that there are 71 Earth co-orbitals larger than 10 m diameter with a lunar provenance at any time.

This number is spuriously close to the 58 known Earth co-orbitals in the same size range. The value is ‘spurious’ because the known population in this size range is incomplete due to observational selection effects which make co-orbitals difficult to detect, especially the smaller ones. Furthermore, the main belt must also supply the Earth co-orbital population and our results suggest that there are about 1600 co-orbitals of a main belt origin, more than  $20\times$  our nominal result for the lunar origin hypothesis. Thus, while the Moon can generate Earth’s co-orbitals it is not necessary to invoke a lunar provenance to explain the known population.

Our classification of the co-orbital regimes of objects with a main belt provenance suggests that about half of them are in tadpole, Trojan-like, orbits, but only 2 are generally recognized while we identified an additional 3 objects. This is most likely an observational selection effect because detecting small Earth Trojans is complicated by their large phase angles and small solar elongations. A population of Earth Trojans would be a valuable source of low  $\Delta v$  asteroids for mining or scientific missions and we predict that the Vera Rubin Observatory will discover many of these objects during a twilight survey.

Assuming the co-orbitals have a main belt provenance predicts that they are dominated by objects from the inner main belt and are therefore primarily taxonomically in the S-complex.

The difference between the number of co-orbitals expected from the main belt and our nominal lunar model, and the uncertainty on the latter population, make it all the more surprising that the colors of some co-orbitals seem to be more consistent with the Moon’s surface than common asteroid taxonomies. If this pattern continues for future spectroscopic observations of the co-orbital population it will indicate that impacts are more efficient at launching ejecta than the nominal parameters employed in our analysis suggest. Measuring the size-frequency distribution of co-orbitals of lunar origin could then constrain impact processes such as crater-scaling relations, ejecta SFDs, and the correlation between ejecta size and speed.

The probability of identifying co-orbitals with spectra similar to the Moon should depend on an object’s eccentricity and inclination with main belt objects dominating the high  $e$  and  $i$  orbital element phase space and lunar ejecta predominant when  $e \rightarrow 0$  and  $i \rightarrow 0^\circ$ . Disentangling the relative contribution of the co-orbital sources will then require debiasing the observations as a function of their orbital elements.

## Acknowledgments

We are grateful to Gabriele Merli and Tommaso del Viscio who helped implement the integrations on the Università di Pavia EOS HPC cluster. E.M. Alessi was supported by the Fondazione Cariplo and the short-term mobility programme of CNR. Uncertainties on all the efficiencies and fractions in histograms and elsewhere were calculated using the technique and software developed by [Paterno \(2004\)](#). This work made extensive use of the NumPy ([Harris et al., 2020](#)), SciPy ([Virtanen et al., 2020](#)), Astropy ([Astropy Collaboration et al., 2013, 2018, 2022](#)) and Matplotlib ([Hunter, 2007](#)) packages. We thank Victoria Coleman for proofreading the original manuscript and Mikael Granvik and an anonymous reviewer for their careful reviews and constructive suggestions to improve this work.

## References

- Astropy Collaboration, T. P. Robitaille, E. J. Tollerud, P. Greenfield, M. Droettboom, E. Bray, T. Aldcroft, M. Davis, A. Ginsburg, A. M. Price-Whelan, W. E. Kerzendorf, A. Conley, N. Crighton, K. Barbary, D. Muna, H. Ferguson, F. Grollier, M. M. Parikh, P. H. Nair, H. M. Unther, C. Deil, J. Woillez, S. Conseil, R. Kramer, J. E. H. Turner, L. Singer, R. Fox, B. A. Weaver, V. Zabalza, Z. I. Edwards, K. Azalee Bostroem, D. J. Burke, A. R. Casey, S. M. Crawford, N. Dencheva, J. Ely, T. Jenness, K. Labrie, P. L. Lim, F. Pierfederici, A. Pontzen, A. Ptak, B. Refsdal, M. Servillat, and O. Streicher. Astropy: A community Python package for astronomy. *A&A*, 558:A33, Oct. 2013. doi: 10.1051/0004-6361/201322068.
- Astropy Collaboration, A. M. Price-Whelan, B. M. Sipócz, H. M. Günther, P. L. Lim, S. M. Crawford, S. Conseil, D. L. Shupe, M. W. Craig, N. Dencheva, A. Ginsburg, J. T. VanderPlas, L. D. Bradley, D. Pérez-Suárez, M. de Val-Borro, T. L. Aldcroft, K. L. Cruz, T. P. Robitaille, E. J. Tollerud, C. Ardelean, T. Babej, Y. P. Bach, M. Bachetti, A. V. Bakanov, S. P. Bamford, G. Barentsen, P. Barmby, A. Baumbach, K. L. Berry, F. Biscani, M. Boquien, K. A. Bostroem, L. G. Bouma, G. B. Brammer, E. M. Bray, H. Breytenbach, H. Buddelmeijer, D. J. Burke, G. Calderone, J. L. Cano Rodríguez, M. Cara, J. V. M. Cardoso, S. Cheedella, Y. Copin, L. Corrales, D. Crichton, D. D’Avella, C. Deil, É. Depagne, J. P. Dietrich, A. Donath, M. Droettboom, N. Earl, T. Erben, S. Fabbro, L. A. Ferreira, T. Finethy, R. T. Fox, L. H. Garrison, S. L. J. Gibbons, D. A. Goldstein, R. Gommers, J. P. Greco, P. Greenfield, A. M. Groener, F. Grollier, A. Hagen, P. Hirst, D. Homeier, A. J. Horton, G. Hosseinzadeh, L. Hu, J. S. Hunkeler, Ž. Ivezić, A. Jain, T. Jenness, G. Kanarek, S. Kendrew, N. S. Kern, W. E. Kerzendorf, A. Khvalko, J. King, D. Kirkby, A. M. Kulkarni, A. Kumar, A. Lee, D. Lenz, S. P. Littlefair, Z. Ma, D. M. Macleod, M. Mastropietro, C. McCully, S. Montagnac, B. M. Morris, M. Mueller, S. J. Mumford, D. Muna, N. A. Murphy, S. Nelson, G. H. Nguyen, J. P. Ninan, M. Nöthe, S. Ogaz, S. Oh, J. K. Parejko, N. Parley, S. Pascual, R. Patil, A. A. Patil, A. L. Plunkett, J. X. Prochaska, T. Rastogi, V. Reddy Janga, J. Sabater, P. Sakurikar, M. Seifert, L. E. Sherbert, H. Sherwood-Taylor, A. Y. Shih, J. Sick, M. T. Silbiger, S. Singanamalla, L. P. Singer, P. H. Sladen, K. A. Sooley, S. Sornarajah, O. Streicher, P. Teuben, S. W. Thomas,

G. R. Tremblay, J. E. H. Turner, V. Terrón, M. H. van Kerkwijk, A. de la Vega, L. L. Watkins, B. A. Weaver, J. B. Whitmore, J. Woillez, V. Zabalza, and Astropy Contributors. The Astropy Project: Building an Open-science Project and Status of the v2.0 Core Package. *AJ*, 156(3):123, Sept. 2018. doi: 10.3847/1538-3881/aabc4f.

Astropy Collaboration, A. M. Price-Whelan, P. L. Lim, N. Earl, N. Starkman, L. Bradley, D. L. Shupe, A. A. Patil, L. Corrales, C. E. Brasseur, M. N"othe, A. Donath, E. Tollerud, B. M. Morris, A. Ginsburg, E. Vaher, B. A. Weaver, J. Tocknell, W. Jamieson, M. H. van Kerkwijk, T. P. Robitaille, B. Merry, M. Bachetti, H. M. G"unther, T. L. Aldcroft, J. A. Alvarado-Montes, A. M. Archibald, A. B'odi, S. Bapat, G. Barentsen, J. Baz'an, M. Biswas, M. Boquien, D. J. Burke, D. Cara, M. Cara, K. E. Conroy, S. Conseil, M. W. Craig, R. M. Cross, K. L. Cruz, F. D'Eugenio, N. Dencheva, H. A. R. Devillepoix, J. P. Dietrich, A. D. Eigenbrot, T. Erben, L. Ferreira, D. Foreman-Mackey, R. Fox, N. Freij, S. Garg, R. Geda, L. Glattly, Y. Gondhalekar, K. D. Gordon, D. Grant, P. Greenfield, A. M. Groener, S. Guest, S. Gurovich, R. Handberg, A. Hart, Z. Hatfield-Dodds, D. Homeier, G. Hosseinzadeh, T. Jenness, C. K. Jones, P. Joseph, J. B. Kalmbach, E. Karamehmetoglu, M. Kaluszy'nski, M. S. P. Kelley, N. Kern, W. E. Kerzendorf, E. W. Koch, S. Kulumani, A. Lee, C. Ly, Z. Ma, C. MacBride, J. M. Maljaars, D. Muna, N. A. Murphy, H. Norman, R. O'Steen, K. A. Oman, C. Pacifici, S. Pascual, J. Pascual-Granado, R. R. Patil, G. I. Perren, T. E. Pickering, T. Rastogi, B. R. Roulston, D. F. Ryan, E. S. Rykoff, J. Sabater, P. Sakurikar, J. Salgado, A. Sanghi, N. Saunders, V. Savchenko, L. Schwaradt, M. Seifert-Eckert, A. Y. Shih, A. S. Jain, G. Shukla, J. Sick, C. Simpson, S. Singanamalla, L. P. Singer, J. Singhal, M. Sinha, B. M. SipHocz, L. R. Spitler, D. Stansby, O. Streicher, J. Sumak, J. D. Swinbank, D. S. Taranu, N. Tewary, G. R. Tremblay, M. d. Val-Borro, S. J. Van Kooten, Z. Vasovi'c, S. Verma, J. V. de Miranda Cardoso, P. K. G. Williams, T. J. Wilson, B. Winkel, W. M. Wood-Vasey, R. Xue, P. Yoachim, C. Zhang, A. Zonca, and Astropy Project Contributors. The Astropy Project: Sustaining and Growing a Community-oriented Open-source Project and the Latest Major Release (v5.0) of the Core Package. *ApJ*, 935(2):167, Aug. 2022. doi: 10.3847/1538-4357/ac7c74.

E. Barrabés and S. Mikkola. Families of periodic horseshoe orbits in the restricted three-body problem. *A&A*, 432:1115–1129, 2005. doi: 10.1051/0004-6361:20041483.

E. Barrabés and M. Ollé. Invariant manifolds of  $L_3$  and horseshoe motion in the restricted three-body problem. *Nonlinearity*, 19:2065–2089, 2006. doi: 10.1088/0951-7715/19/9/004.

G. D. Bart and H. J. Melosh. Distributions of boulders ejected from lunar craters. *Icarus*, 209(2):337–357, October 2010. doi: 10.1016/j.icarus.2010.05.023.

A. Bengochea, M. Falconi, and E. Pérez-Chavela. Horseshoe periodic orbits with one symmetry in the general planar three-body problem. *Discrete Contin. Dyn. Syst.*, 33(3): 987–1008, 2013.

R. P. Binzel, A. Morbidelli, S. Merouane, F. E. DeMeo, M. Birlan, P. Vernazza, C. A. Thomas, A. S. Rivkin, S. J. Bus, and A. T. Tokunaga. Earth encounters as the origin

- of fresh surfaces on near-Earth asteroids. *Nature*, 463(7279):331–334, Jan. 2010. doi: 10.1038/nature08709.
- M. Birlan, O. Vaduvescu, A. Tudorica, A. Sonka, A. Nedelcu, A. Galad, F. Colas, F. Pozo N., A. Barr D., R. Toma, I. Comsa, P. Rocher, V. Lainey, D. Vidican, D. Asher, C. Opriseanu, C. Vancea, J. P. Colque, C. P. Soto, R. Rekola, and E. Unda-Sanzana. More than 160 near Earth asteroids observed in the EURONEAR network. *A&A*, 511:A40, Feb. 2010. doi: 10.1051/0004-6361/200912865.
- B. T. Bolin, C. Fremling, T. R. Holt, M. J. Hankins, T. Ahumada, S. Anand, V. Bhalerao, K. B. Burdge, C. M. Copperwheat, M. Coughlin, K. P. Deshmukh, K. De, M. M. Kasliwal, A. Morbidelli, J. N. Purdum, R. Quimby, D. Bodewits, C.-K. Chang, W.-H. Ip, C.-Y. Hsu, R. R. Laher, Z.-Y. Lin, C. M. Lisse, F. J. Masci, C.-C. Ngeow, H. Tan, C. Zhai, R. Burruss, R. Dekany, A. Delacroix, D. A. Duev, M. Graham, D. Hale, S. R. Kulkarni, T. Kupfer, A. Mahabal, P. J. Mróz, J. D. Neill, R. Riddle, H. Rodriguez, R. M. Smith, M. T. Soumagnac, R. Walters, L. Yan, and J. Zolkower. Characterization of Temporarily Captured Minimoons 2020 CD<sub>3</sub> by Keck Time-resolved Spectrophotometry. *ApJ*, 900(2): L45, Sept. 2020. doi: 10.3847/2041-8213/abae69.
- B. T. Bolin, L. Denneau, L.-M. Abron, R. Jedicke, K. Chiboucas, C. Ingebreetsen, and B. C. Lemaux. The Discovery and Characterization of Minimoons 2024 PT<sub>5</sub>. *ApJ*, 978(2):L37, Jan. 2025a. doi: 10.3847/2041-8213/ada1d0.
- B. T. Bolin, F. J. Masci, M. W. Coughlin, D. A. Duev, Ž. Ivezić, R. L. Jones, P. Yoachim, T. Ahumada, V. Bhalerao, H. Choudhary, C. Contreras, Y.-C. Cheng, C. M. Copperwheat, K. Deshmukh, C. Fremling, M. Granvik, K. K. Hardegree-Ullman, A. Y. Q. Ho, R. Jedicke, M. Kasliwal, H. Kumar, Z.-Y. Lin, A. Mahabal, A. Monson, J. D. Neill, D. Nesvorný, D. A. Perley, J. N. Purdum, R. Quimby, E. Serabyn, K. Sharma, and V. Swain. The Palomar twilight survey of 'Ayló'chaxnim, Atiras, and comets. *Icarus*, 425: 116333, Jan. 2025b. doi: 10.1016/j.icarus.2024.116333.
- G. B. Borisov, A. A. Christou, and G. Apostolovska. Physical and dynamical properties of selected Earth co-orbital asteroids. *Planet. Space Sci.*, 225:105619, Jan. 2023. doi: 10.1016/j.pss.2022.105619.
- W. F. Bottke, D. Vokrouhlicky, B. Ghent, S. Mazrouei, S. Robbins, and S. Marchi. On asteroid impacts, crater scaling laws, and a proposed younger surface age for venus. In *47th Lunar and Planetary Science Conference*, page Abstract #2036, Houston, 2016. Lunar and Planetary Institute. URL <https://www.hou.usra.edu/meetings/lpsc2016/pdf/2036.pdf>.
- R. Brassier, K. Innanen, M. Connors, C. Veillet, P. Wiegert, S. Mikkola, and P. Chodas. Transient co-orbital asteroids. *Icarus*, 171(1):102–109, 2004.
- E. W. Brown. Orbits, Periodic, On a new family of periodic orbits in the problem of three bodies. *Monthly Notices of the RAS*, 71:438–454, 1911.

- J. D. Castro-Cisneros, R. Malhotra, and A. J. Rosengren. Lunar ejecta origin of near-Earth asteroid Kamo'oaewa is compatible with rare orbital pathways. *Communications Earth and Environment*, 4(1):372, Dec. 2023. doi: 10.1038/s43247-023-01031-w.
- A. A. Christou. A Numerical Survey of Transient Co-orbitals of the Terrestrial Planets. *Icarus*, 144:1–20, 2000.
- A. A. Christou. Orbital clustering of martian trojans: An asteroid family in the inner solar system? *Icarus*, 224(1):144–153, 2013. ISSN 0019-1035. doi: 10.1016/j.icarus.2013.02.013.
- S. Cicalò, E. M. Alessi, L. Provinciali, et al. Mission analysis for the HENON CubeSat mission to a large Sun-Earth distant retrograde orbit. *Astrophys Space Sci*, 370(83), 2025. doi: 10.1007/s10509-025-04473-0.
- G. S. Collins, H. J. Melosh, and R. A. Marcus. Earth impact effects program: A web-based computer program for calculating the regional environmental consequences of a meteoroid impact on earth. *Meteoritics & Planetary Science*, 40(6):817–840, 2005. doi: <https://doi.org/10.1111/j.1945-5100.2005.tb00157.x>. URL <https://onlinelibrary.wiley.com/doi/abs/10.1111/j.1945-5100.2005.tb00157.x>.
- M. Connors. A Kozai-resonating Earth quasi-satellite. *MNRAS*, 437(1):L85–L89, Jan. 2014. doi: 10.1093/mnrasl/slt147.
- J. M. Cors, J. F. Palacián, and P. Yanguas. On co-orbital quasi-periodic motion in the three-body problem. *SIAM J. Appl. Dyn. Syst.*, 18(1):334–353, 2019.
- F. Cortese, S. Di Ruzza, and E. M. Alessi. A statistical sparse jump model for automatic identification of dynamical transitions in the co-orbital regime. *Nonlinear Dynamics*, 2025. doi: 10.1007/s11071-025-11171-7.
- C. de la Fuente Marcos and R. de la Fuente Marcos. (309239) 2007 RW10: a large temporary quasi-satellite of Neptune. *Astronomy & Astrophysics*, 549:L9, 2012. doi: 10.1051/0004-6361/201219931.
- C. de la Fuente Marcos and R. de la Fuente Marcos. Asteroid 2014 YX49: a large transient Trojan of Uranus. *Monthly Notices of the Royal Astronomical Society*, 467(2):1561–1568, 01 2017. ISSN 0035-8711. doi: 10.1093/mnras/stx197. URL <https://doi.org/10.1093/mnras/stx197>.
- F. E. DeMeo and B. Carry. Solar System evolution from compositional mapping of the asteroid belt. *Nature*, 505:629–634, January 2014. doi: 10.1038/nature12908.
- F. E. DeMeo, R. P. Binzel, and M. Lockhart. Mars encounters cause fresh surfaces on some near-Earth asteroids. *Icarus*, 227:112–122, Jan. 2014. doi: 10.1016/j.icarus.2013.09.014.

- L. Denneau, R. Jedicke, T. Grav, M. Granvik, J. Kubica, A. Milani, P. Vereš, R. Wainscoat, D. Chang, F. Pierfederici, N. Kaiser, K. C. Chambers, J. N. Heasley, E. A. Magnier, P. A. Price, J. Myers, J. Kleyna, H. Hsieh, D. Farnocchia, C. Waters, W. H. Sweeney, D. Green, B. Bolin, W. S. Burgett, J. S. Morgan, J. L. Tonry, K. W. Hodapp, S. Chastel, S. Chesley, A. Fitzsimmons, M. Holman, T. Spahr, D. Tholen, G. V. Williams, S. Abe, J. D. Armstrong, T. H. Bressi, R. Holmes, T. Lister, R. S. McMillan, M. Micheli, E. V. Ryan, W. H. Ryan, and J. V. Scotti. The Pan-STARRS Moving Object Processing System. *PASP*, 125:357–395, April 2013. doi: 10.1086/670337.
- S. F. Dermott and C. D. Murray. The dynamics of tadpole and horseshoe orbits II. The coorbital satellites of saturn. *Icarus*, 48:12–22, 1981.
- S. Di Ruzza, A. Pousse, and E. M. Alessi. On the co-orbital asteroids in the solar system: medium-term timescale analysis of the quasi-coplanar objects. *Icarus*, 390:115330, January 2023. doi: 10.1016/j.icarus.2022.115330.
- J. S. Dohnanyi. Collisional Model of Asteroids and Their Debris. *J. Geophys. Res.*, 74: 2531–2554, May 1969. doi: 10.1029/JB074i010p02531.
- G. Fedorets, M. Granvik, and R. Jedicke. Orbit and size distributions for asteroids temporarily captured by the Earth-Moon system. *Icarus*, 285:83–94, March 2017. doi: 10.1016/j.icarus.2016.12.022.
- G. Fedorets, M. Micheli, R. Jedicke, S. P. Naidu, D. Farnocchia, M. Granvik, N. Moskovitz, M. E. Schwamb, R. Weryk, K. Wierzchoś, E. Christensen, T. Pruyne, W. F. Bottke, Q. Ye, R. Wainscoat, M. Devogèle, L. E. Buchanan, A. A. Djupvik, D. M. Faes, D. Föhring, J. Roediger, T. Secull, and A. B. Smith. Establishing Earth’s Minimoons Population through Characterization of Asteroid 2020 CD<sub>3</sub>. *AJ*, 160(6):277, Dec. 2020. doi: 10.3847/1538-3881/abc3bc.
- M. Fenucci, B. Novaković, M. Granvik, and P. Zhang. Origin of asteroid (469219) Kamo‘oalewa: the main asteroid belt or the Giordano Bruno crater on the Moon? *arXiv e-prints*, art. arXiv:2601.08923, Jan. 2026.
- M. A. Galiazzo and R. Schwarz. The Hungaria region as a possible source of Trojans and satellites in the inner Solar system. *MNRAS*, 445(4):3999–4007, Dec. 2014. doi: 10.1093/mnras/stu2016.
- B. J. Gladman, F. Migliorini, A. Morbidelli, V. Zappala, P. Michel, A. Cellino, C. Froeschle, H. F. Levison, M. Bailey, and M. Duncan. Dynamical lifetimes of objects injected into asteroid belt resonances. *Science*, 277:197–201, January 1997. doi: 10.1126/science.277.5323.197.
- G. Gómez, À. Jorba, C. Simó, and J. Masdemont. *Dynamics and Mission Design Near Libration Points. Volume IV: Advanced Methods for Triangular Points*. WORLD SCIENTIFIC, 2001. doi: 10.1142/4336.

- M. Granvik and K. J. Walsh. Tidal Disruption of Near-Earth Asteroids during Close Encounters with Terrestrial Planets. *ApJ*, 960(2):L9, Jan. 2024. doi: 10.3847/2041-8213/ad151b.
- M. Granvik, J. Vaubaillon, and R. Jedicke. The population of natural Earth satellites. *Icarus*, 218:262–277, March 2012. doi: 10.1016/j.icarus.2011.12.003.
- M. Granvik, R. Jedicke, B. Bolin, M. Chyba, G. Patterson, and G. Picot. *Earth’s Temporarily-Captured Natural Satellites - The First Step towards Utilization of Asteroid Resources*, pages 151–167. 2013. doi: 10.1007/978-3-642-39244-3\_6.
- M. Granvik, A. Morbidelli, R. Jedicke, B. Bolin, W. F. Bottke, E. Beshore, D. Vokrouhlický, D. Nesvorný, and P. Michel. Debiased orbit and absolute-magnitude distributions for near-Earth objects. *Icarus*, 312:181–207, Sept. 2018. doi: 10.1016/j.icarus.2018.04.018.
- S. Greenstreet, B. Gladman, and M. Jurić. Jupiter’s Metastable Companions. *The Astrophysical Journal Letters*, 963:L40, 2024. doi: 10.3847/2041-8213/ad28c5.
- C. R. Harris, K. J. Millman, S. J. van der Walt, R. Gommers, P. Virtanen, D. Cournapeau, E. Wieser, J. Taylor, S. Berg, N. J. Smith, R. Kern, M. Picus, S. Hoyer, M. H. van Kerkwijk, M. Brett, A. Haldane, J. F. del Río, M. Wiebe, P. Peterson, P. Gérard-Marchant, K. Sheppard, T. Reddy, W. Weckesser, H. Abbasi, C. Gohlke, and T. E. Oliphant. Array programming with NumPy. *Nature*, 585(7825):357–362, Sept. 2020. doi: 10.1038/s41586-020-2649-2. URL <https://doi.org/10.1038/s41586-020-2649-2>.
- G. P. Horedt and G. Neukum. Comparison of six crater-scaling laws. *Earth Moon and Planets*, 31:265–269, December 1984. doi: 10.1007/BF00058905.
- K. R. Housen and K. A. Holsapple. Ejecta from impact craters. *Icarus*, 211(1):856–875, January 2011. doi: 10.1016/j.icarus.2010.09.017.
- M. Hui, P. Wiegert, R. Weryk, et al. 2019 UO<sub>19</sub>: A Transient Trojan of Saturn. *The Astronomical Journal Letters*, 975:L3, 2024. doi: 10.3847/2041-8213/ad84ef.
- M.-T. Hui, P. A. Wiegert, D. J. Tholen, and D. Föhring. The Second Earth Trojan 2020 XL<sub>5</sub>. *The Astrophysical Journal Letters*, 922:L25, 2021. doi: 10.3847/2041-8213/ac37bf.
- J. D. Hunter. Matplotlib: A 2d graphics environment. *Computing in Science & Engineering*, 9(3):90–95, 2007. doi: 10.1109/MCSE.2007.55.
- R. Jedicke, D. Nesvorný, R. Whiteley, Ž. Ivezić, and M. Jurić. An age-colour relationship for main-belt S-complex asteroids. *Nature*, 429(6989):275–277, May 2004. doi: 10.1038/nature02578.
- R. Jedicke, J. Sercel, J. Gillis-Davis, K. J. Morenz, and L. Gertsch. Availability and delta-v requirements for delivering water extracted from near-Earth objects to cis-lunar space. *Planet. Space Sci.*, 159:28–42, Sept. 2018. doi: 10.1016/j.pss.2018.04.005.

- R. Jedicke, E. M. Alessi, N. Wiedner, M. Ghosal, E. B. Bierhaus, and M. Granvik. The steady state population of earth’s minimoons of lunar provenance. *Icarus*, 438:116587, 2025. doi: 10.1016/j.icarus.2025.116587.
- Y. Jiao, B. Cheng, Y. Huang, E. Asphaug, B. Gladman, R. Malhotra, P. Michel, Y. Yu, and H. Baoyin. Asteroid Kamo’oalewa’s journey from the lunar Giordano Bruno crater to Earth 1:1 resonance. *Nature Astronomy*, 8:819–826, July 2024. doi: 10.1038/s41550-024-02258-z.
- M. Jorba-Cuscó and R. Epenoy. Low-fuel transfers from Mars to quasi-satellite orbits around Phobos exploiting manifolds of tori. *Celestial Mechanics and Dynamical Astronomy*, 133:20, 2021. doi: 10.1007/s10569-021-10017-9.
- M. Kaplan and S. Cengiz. Horseshoe co-orbitals of Earth: current population and new candidates. *MNRAS*, 496(4):4420–4432, Aug. 2020. doi: 10.1093/mnras/staa1873.
- T. Kareta, O. Fuentes-Muñoz, N. Moskovitz, D. Farnocchia, and B. N. L. Sharkey. On the Lunar Origin of Near-Earth Asteroid 2024 PT5. *ApJ*, 979(1):L8, Jan. 2025. doi: 10.3847/2041-8213/ad9ea8.
- H. Kinoshita and H. Nakai. Quasi-satellites of Jupiter. *Celestial Mechanics and Dynamical Astronomy*, 98:181–189, 2007. doi: 10.1007/s10569-007-9074-9.
- M. Lavagna, E. Belloni, F. De Cecio, A. Dottori, G. Zanotti, J. Brucato, F. Fiore, A. Meneghin, M. Amoroso, A. Fedele, and S. Natalucci. CubeSat paradigm exploitation for Deimos moon scientific investigation: the taste mission phase B activities. In *75th International Astronautical Congress (IAC)*, 2024. Paper IAC-24,A3,4B,9.
- J. Li, Z. J. Xia, F. Yoshida, N. Georgakarakos, and X. Li. Asymmetry in the number of L4 and L5 Jupiter Trojans driven by jumping Jupiter. *A&A*, 669:A68, 2023. doi: 10.1051/0004-6361/202244443.
- J. Llibre and M. Ollé. The motion of saturn coorbital satellites in the restricted three-body problem. *Astronomy and Astrophysics*, 378:1087–1099, 2001.
- S. Mikkola and K. Innanen. Orbital stability of planetary quasi-satellites. In *Dvorak, R., Henrard, J. (eds.) The Dynamical Behaviour of our Planetary System*, Kluwer Academic Publishers, page 345, 1997.
- S. Mikkola, K. Innanen, K. Muinonen, and E. Bowell. A preliminary analysis of the orbit of the Mars Trojan asteroid (5261) Eureka. *Celestial Mechanics and Dynamical Astronomy*, 58:53–64, 1994. doi: 10.1007/BF00692117.
- S. Mikkola, R. Brasser, P. Wiegert, and K. Innanen. Asteroid 2022 VE68, a quasi-satellite of Venus. *Monthly Notices of the Royal Astronomical Society*, 351:L63–L65, 2004. doi: 10.1111/j.1365-2966.2004.07994.x.

- M. H. M. Morais and A. Morbidelli. The population of Near-Earth Asteroids in coorbital motion with the Earth. *Icarus*, 160:1–9, 2002. doi: 10.1016/j.icarus.2002.6937.
- M. H. M. Morais and F. Namouni. Asteroids in retrograde resonance with Jupiter and Saturn. *MNRAS*, 436:L30–L34, Nov. 2013a. doi: 10.1093/mnras/slt106.
- M. H. M. Morais and F. Namouni. Retrograde resonance in the planar three-body problem. *Celestial Mechanics and Dynamical Astronomy*, 117(4):405–421, Dec. 2013b. doi: 10.1007/s10569-013-9519-2.
- T. Morota, J. Haruyama, H. Miyamoto, C. Honda, M. Ohtake, Y. Yokota, T. Matsunaga, N. Hirata, H. Demura, H. Takeda, Y. Ogawa, and J. Kimura. Formation age of the lunar crater Giordano Bruno. *M&PS*, 44(8):1115–1120, Aug. 2009. doi: 10.1111/j.1945-5100.2009.tb01211.x.
- F. Namouni. Secular interactions of coorbiting objects. *Icarus*, 137(2):293–314, 1999.
- D. Nesvorný and D. Vokrouhlický. Chaotic capture of Neptune Trojans. *The Astronomical Journal*, 137:5003, 2009. doi: 10.1088/0004-6256/137/6/5003.
- D. Nesvorný, D. Vokrouhlický, F. Shelly, R. Deienno, W. F. Bottke, C. Fuls, R. Jedicke, S. Naidu, S. R. Chesley, P. W. Chodas, D. Farnocchia, and M. Delbo. NEOMOD 3: The debiased size distribution of Near Earth Objects. *Icarus*, 417:116110, July 2024. doi: 10.1016/j.icarus.2024.116110.
- N. Ogawa, Y. T. Tsuda, Y. Takei, H. Inoue, S. Takahashi, and Y. Kawakatsu. Orbit Design for the Martian Moons Exploration Mission. *Transactions of the Japan Society for the Aeronautical and Space Sciences, Aerospace Technology Japan*, 17(3):398–403, 2019. doi: 10.2322/tastj.17.398.
- N. Pan and T. Gallardo. An attempt to build a dynamical catalog of present-day solar system co-orbitals. *Celestial Mechanics and Dynamical Astronomy*, 137:2, 2025. doi: 10.1007/s10569-024-10234-y.
- M. Paterno. *Calculating efficiencies and their uncertainties*. United States. Department of Energy, 2004.
- D. Polishook, S. Jacobson, A. Morbidelli, et al. A Martian origin for the Mars Trojan asteroids. *Nature Astronomy*, 1:0179, 2017. doi: 10.1038/s41550-017-0179.
- A. Pousse and E. M. Alessi. Revisiting the averaged problem in the case of mean-motion resonances in the restricted three-body problem. *Nonlinear Dynamics*, 108:959–985, 2022. doi: 10.1007/s11071-022-07229-5.
- A. Pousse, P. Robutel, and A. Vienne. On the co-orbital motion in the planar restricted three-body problem: the quasi-satellite motion revisited. *Celestial Mechanics and Dynamical Astronomy*, 128(4):383–407, 2017. doi: 10.1007/s10569-016-9749-1.

- E. Rabe. Determination and survey of periodic Trojan orbits in the restricted problem of three bodies. *Astronomical Journal*, 66:500, 1961.
- H. Rein and S. F. Liu. REBOUND: an open-source multi-purpose N-body code for collisional dynamics. *A&A*, 537:A128, 2012. doi: 10.1051/0004-6361/201118085.
- P. Robutel and A. Pousse. On the co-orbital motion of two planets in quasi-circular orbits. *Celest. Mech. Dyn. Astron.*, 117:17–40, 2013.
- P. Robutel, F. Gabern, and À. Jorba. The Observed Trojans and the Global Dynamics Around The Lagrangian Points of the Sun–Jupiter System. *Celestial Mechanics and Dynamical Astronomy*, 92:53–69, 2005. doi: 10.1007/s10569-004-5976-y.
- T. Santana-Ros, M. Micheli, L. Faggioli, R. Cennamo, M. Devogèle, A. Alvarez-Candal, D. Oszkiewicz, O. Ramórez, P. Liu, P. Benavidez, A. Campo Bagatin, E. Christensen, R. Wainscoat, L. Weryk, R. and Fraga, C. Briceño, and L. Conversi. Orbital stability analysis and photometric characterization of the second Earth Trojan asteroid 2020 XL5. *Nature Communications*, 13:447, 2022.
- H. Scholl, F. Marzari, and P. Tricarico. The instability of Venus Trojans. *The Astronomical Journal*, 130:2912–2915, 2005.
- M. E. Schwamb, R. L. Jones, P. Yoachim, K. Volk, R. C. Dorsey, C. Opitom, S. Greenstreet, T. Lister, C. Snodgrass, B. T. Bolin, L. Inno, M. T. Bannister, S. Eggl, M. Solontoi, M. S. P. Kelley, M. Jurić, H. W. Lin, D. Ragozzine, P. H. Bernardinelli, S. R. Chesley, T. Daylan, J. Durech, W. C. Fraser, M. Granvik, M. M. Knight, C. M. Lisse, R. Malhotra, W. J. Oldroyd, A. Thirouin, and Q. Ye. Tuning the Legacy Survey of Space and Time (LSST) Observing Strategy for Solar System Science. *ApJS*, 266(2):22, June 2023. doi: 10.3847/1538-4365/acc173.
- R. Sfair, L. C. Gomes, O. C. Winter, R. A. Moraes, G. Borderes-Motta, and C. M. Schäfer. The Moon as a possible source for Earth’s co-orbital bodies. *arXiv:2505.09066v1*, 2025. doi: 0.48550/arXiv.2505.09066.
- B. N. L. Sharkey, V. Reddy, R. Malhotra, A. Thirouin, O. Kuhn, A. Conrad, B. Rothberg, J. A. Sanchez, D. Thompson, and C. Veillet. Lunar-like silicate material forms the Earth quasi-satellite (469219) 2016 HO3 Kamo‘oalewa. *Communications Earth & Environment*, 2(1):231, 2021. doi: 10.1038/s43247-021-00303-7.
- K. N. Singer, B. L. Jolliff, and W. B. McKinnon. Lunar Secondary Craters and Estimated Ejecta Block Sizes Reveal a Scale-Dependent Fragmentation Trend. *Journal of Geophysical Research (Planets)*, 125(8):e06313, August 2020. doi: 10.1029/2019JE006313.
- F. Spirig and J. Waldvogel. The three-body problem with two small masses - a singular-perturbation approach to the problem of saturn’s coorbiting satellites. In *Szebehely, V. G., editor, NATO (ASI) Series C*, 154:53–63, 1985.

- E. Strömberg. Connaissance actuelle des orbites dans le problème des trois corps. *Bulletin Astronomique, Mémoires et variétés*, 9:87–130, 1933. doi: 10.3406/bastr.1933.14090.
- V. Szebehely. *Theory of Orbits*. Academic Press, 1967. doi: 10.1016/B978-0-12-395732-0.X5001-6.
- C. Tardioli, D. Farnocchia, B. Rozitis, D. Cotto-Figueroa, S. R. Chesley, T. S. Statler, and M. Vasile. Constraints on the near-Earth asteroid obliquity distribution from the Yarkovsky effect. *A&A*, 608:A61, Dec. 2017. doi: 10.1051/0004-6361/201731338.
- P. Virtanen, R. Gommers, T. E. Oliphant, M. Haberland, T. Reddy, D. Cournapeau, E. Burovski, P. Peterson, W. Weckesser, J. Bright, S. J. van der Walt, M. Brett, J. Wilson, K. J. Millman, N. Mayorov, A. R. J. Nelson, E. Jones, R. Kern, E. Larson, C. J. Carey, Í. Polat, Y. Feng, E. W. Moore, J. VanderPlas, D. Laxalde, J. Perktold, R. Cimrman, I. Henriksen, E. A. Quintero, C. R. Harris, A. M. Archibald, A. H. Ribeiro, F. Pedregosa, P. van Mulbregt, and SciPy 1.0 Contributors. SciPy 1.0: Fundamental Algorithms for Scientific Computing in Python. *Nature Methods*, 17:261–272, 2020. doi: 10.1038/s41592-019-0686-2.
- G. Voyatzis and K. I. Antoniadou. On quasi-satellite periodic motion in asteroid and planetary dynamics. *Celestial Mechanics and Dynamical Astronomy*, 130:59, 2018. doi: 10.1007/s10569-018-9856-2.
- P. Wajer. Dynamical evolution of Earth’s quasi-satellites: 2004 GU9 and 2006 FV35. *Icarus*, 209:488–493, 2010. doi: 10.1016/j.icarus.2010.05.012.
- P. Wiegert, M. Connors, and C. Veillet. A retrograde co-orbital asteroid of Jupiter. *Nature*, 543:687–689, 2017. doi: 10.1038/nature22029.
- P. A. Wiegert, K. A. Innanen, and S. Mikkola. An asteroidal companion to the Earth. *nat*, 387:685–686, 1997.
- Y. Wu, Y. Jiao, W.-Y. Dai, Y. Huang, Z. Liu, B. Cheng, H. Baoyin, and J. Li. Detectability of Lunar-origin Asteroids in the LSST Era. *ApJ*, 997(2):354, Feb. 2026. doi: 10.3847/1538-4357/ae2eab.
- C. F. Yoder, G. Colombo, S. P. Synnott, and K. A. Yoder. Theory of motion of saturn’s coorbiting satellites. *Icarus*, 53:431–443, 1983.
- P. F. Zhang, Y. Li, G. Z. Zhang, X. R. Yan, Y. X. Zhang, P. Vernazza, E. A. Cloutis, T. Hiroi, M. Granvik, X. P. Zhang, and Y. T. Lin. (469219) Kamo‘oalewa, A Space-Weathering-Matured Old-Age LL-Chondrite-Like Small NEA: Target of the Tianwen-2 Sample Return Mission. In *55th Lunar and Planetary Science Conference*, volume 3040 of *LPI Contributions*, page 1845, Mar. 2024.

- R. Zhang, H. Zhang, J. Liu, Y. Geng, L. Meng, H. Li, T. Yu, and C. Xue. Tianwen-2 small bodies exploration mission. *Scientia Sinica Physica, Mechanica & Astronomica*, 55(7): 279501, Jan. 2025. doi: 10.1360/SSPMA-2025-0083.
- T. Zhang, X. Kun, and D. Xilun. China’s ambitions and challenges for asteroid–comet exploration. *Nature Astronomy*, 5:730–731, 2021. doi: 10.1038/s41550-021-01418-9.
- M.-H. Zhu, A. Morbidelli, Z. Wei, P. Ma, M. Ding, X.-Z. Luo, H. Zhang, L. Xu, Y. Zhuang, and X.-L. Cui. Lunar origin of earth quasi-satellite kamo’oalewa. *The Innovation*, page 101183, 2025. ISSN 2666-6758. doi: 10.1016/j.xinn.2025.101183. URL <https://www.sciencedirect.com/science/article/pii/S2666675825003868>.

## Appendix - Known Earth co-orbitals

Table A.1: Known asteroids that are currently Earth co-orbitals sorted by their designations. JD is the nearest Julian date to the current date that the object had semi-major axis  $a = 1$ . The eccentricity,  $e$ , and inclination,  $i$  are provided at JD. (469219) Kamo‘oalewa is 2016 HO<sub>3</sub>. The bold face initialism in the last column represents the co-orbital regime that the object currently occupies and the other initialisms indicate others that the object experiences during the period of the study from 1600-2500.

JD	$e$	$i$ [deg]	designation	co-orbital regime
2415948.96	0.51	19.79	1986 TO	<b>CP</b>
2447165.65	0.35	33.14	1998 UP <sub>1</sub>	<b>CP</b>
2452475.70	0.23	1.95	2000 PH <sub>5</sub>	<b>HS</b> + CP
2452001.06	0.17	4.67	2001 GO <sub>2</sub>	<b>HS</b> + QS
2452550.15	0.01	10.74	2002 AA <sub>29</sub>	<b>HS</b>
2451752.57	0.04	4.29	2003 YN <sub>107</sub>	<b>HS</b> + QS
2464634.68	0.14	13.66	2004 GU <sub>9</sub>	<b>QS</b>
2445884.10	0.63	2.66	2005 UH <sub>6</sub>	<b>TP</b> + HS
2453979.84	0.30	33.94	2005 QQ <sub>87</sub>	<b>TP</b>
2447416.15	0.38	7.11	2006 FV <sub>35</sub>	<b>QS</b>
2454205.02	0.27	1.52	2009 HE <sub>60</sub>	<b>HS</b> + QS
2455112.23	0.09	6.84	2009 SH <sub>2</sub>	<b>CP</b>
2458292.93	0.37	11.67	2010 NY <sub>65</sub>	<b>CP</b>
2455182.20	0.08	14.54	2010 SO <sub>16</sub>	<b>HS</b>
2456673.65	0.19	20.89	2010 TK <sub>7</sub>	<b>TP</b>
2473934.91	0.03	0.90	2011 UD <sub>21</sub>	<b>HS</b> + CP
2456338.41	0.09	0.82	2013 BS <sub>45</sub>	<b>HS</b>
2522684.91	0.45	50.06	2013 LX <sub>28</sub>	<b>QS</b>
2454673.18	0.46	10.19	2014 OL <sub>339</sub>	<b>QS</b> + HS
2457295.21	0.11	9.20	2015 SO <sub>2</sub>	<b>HS</b> + QS
2457370.22	0.28	1.78	2015 YA	<b>QS</b> + HS
2457381.44	0.41	2.50	2015 YQ <sub>1</sub>	<b>CP</b>
2457734.05	0.18	7.69	2015 XX <sub>169</sub>	<b>CP</b>
2458132.16	0.13	6.39	2016 CO <sub>246</sub>	<b>CP</b>
2458888.70	0.05	27.73	2016 CA <sub>138</sub>	<b>HS</b>
2462506.41	0.10	7.81	2016 HO <sub>3</sub>	<b>QS</b> + HS
2473372.23	0.27	0.09	2016 JA	<b>HS</b>
2457810.31	0.24	2.99	2017 DR <sub>109</sub>	<b>CP</b>
2457833.43	0.27	1.73	2017 FZ <sub>2</sub>	<b>QS</b> + HS
2458746.73	0.15	8.73	2017 SL <sub>16</sub>	<b>CP</b>
2458840.54	0.21	27.21	2017 XQ <sub>60</sub>	<b>CP</b>
2457039.55	0.15	22.10	2018 AN <sub>2</sub>	<b>CP</b>
2456718.64	0.03	4.40	2018 PN <sub>22</sub>	<b>HS</b> + QS

Continued on next page

**Table A.1 continued from previous page**

JD	$e$	$i$ [deg]	designation	co-orbital regimes
2457896.31	0.20	9.14	2018 KS	<b>CP</b>
2457367.46	0.30	19.68	2018 XW <sub>2</sub>	<b>CP</b>
2437143.40	0.04	1.84	2019 GF <sub>1</sub>	<b>HS</b>
2462423.17	0.07	6.70	2019 GM <sub>1</sub>	<b>QS</b> + HS
2458763.88	0.27	7.21	2019 SB <sub>6</sub>	<b>CP</b>
2459616.43	0.28	1.66	2019 VL <sub>5</sub>	<b>HS</b>
2428282.14	0.33	4.20	2019 XS	<b>CP</b> + TP
2458851.98	0.19	0.47	2019 YB <sub>4</sub>	<b>HS</b>
2459265.91	0.16	12.76	2020 CX <sub>1</sub>	<b>CP</b>
2441019.79	0.06	5.80	2020 PP <sub>1</sub>	<b>HS</b> + QS
2459453.40	0.13	4.95	2020 PN <sub>1</sub>	<b>CP</b>
2449742.78	0.39	13.85	2020 XL <sub>5</sub>	<b>TP</b>
2459231.76	0.23	12.52	2021 BA	<b>CP</b>
2459359.91	0.02	2.99	2021 LF <sub>6</sub>	<b>CP</b> + HS + QS
2459547.63	0.32	6.79	2021 XV	<b>CP</b>
2459875.28	0.26	2.12	2022 UX <sub>1</sub>	<b>HS</b> + QS
2459880.55	0.11	6.78	2022 UU <sub>8</sub>	<b>CP</b> + QS + HS
2459541.38	0.17	5.63	2022 VR <sub>1</sub>	<b>CP</b>
2459936.23	0.20	2.36	2022 YG	<b>QS</b> + CP
2443967.77	0.45	7.00	2022 YF <sub>4</sub>	<b>CP</b>
2460021.36	0.18	2.75	2023 FW <sub>13</sub>	<b>QS</b>
2460380.09	0.15	6.87	2023 GC <sub>2</sub>	<b>CP</b>
2460173.72	0.15	4.74	2023 QR <sub>1</sub>	<b>CP</b>
2460194.07	0.15	3.53	2023 SP <sub>2</sub>	<b>CP</b>
2460249.14	0.22	4.49	2023 TG <sub>14</sub>	<b>CP</b>
2460312.27	0.25	5.76	2024 AV <sub>2</sub>	<b>CP</b> + TP + HS
2463025.05	0.35	5.94	2024 JR <sub>16</sub>	<b>TP</b>
2460713.48	0.13	4.44	2025 CJ	<b>CP</b>
2461054.12	0.11	11.87	2025 BL	<b>QS</b> + HS
2466179.17	0.27	11.00	2025 FP <sub>4</sub>	<b>CP</b>
2455872.27	0.17	4.54	2025 KR <sub>4</sub>	<b>CP</b>
2461238.24	0.11	1.99	2025 PN <sub>7</sub>	<b>QS</b> + HS
2452137.80	0.29	16.65	2025 RB <sub>7</sub>	<b>CP</b>
2460936.40	0.10	3.55	2025 SC	<b>QS</b> + CP + HS

JD	$e$	$i$ (deg)	designation	co-orbital regime
2395963.76	0.20	2.14	2002 VX <sub>91</sub>	HS + CP
2507115.77	0.33	1.39	2008 NP <sub>3</sub>	CP
2524681.26	0.03	1.78	2010 VQ <sub>98</sub>	HS + QS
2386261.35	0.04	2.31	2013 RZ <sub>53</sub>	HS
2429919.90	0.02	8.20	2014 UR	CP
2484521.14	0.32	0.91	2015 XF <sub>261</sub>	QS
2530606.45	0.33	0.43	2018 UC	HS
2433929.49	0.12	1.70	2019 DJ <sub>1</sub>	HS + CP
2592075.39	0.01	5.97	2019 HM	HS
2493516.17	0.15	4.10	2019 XH <sub>2</sub>	CP
2436661.34	0.21	0.94	2020 FN <sub>3</sub>	HS
2482335.34	0.02	4.73	2020 HO <sub>5</sub>	CP
2517726.61	0.46	5.97	2021 EY <sub>1</sub>	CP
2418282.93	0.26	0.82	2021 JE <sub>1</sub>	HS
2531392.10	0.02	3.09	2022 RW <sub>3</sub>	QS + HS
2477458.62	0.04	1.86	2023 HM <sub>4</sub>	CP
2415098.45	0.19	4.72	2023 OU	CP
2528508.64	0.05	8.00	2023 RA <sub>10</sub>	CP
2524679.73	0.04	2.24	2023 RX <sub>1</sub>	HS
2493474.60	0.09	2.87	2023 SO <sub>11</sub>	HS + QS
2408554.79	0.34	13.97	2024 HB	CP
2583032.67	0.02	0.92	2024 PT <sub>5</sub>	HS
2492505.82	0.06	4.65	2025 DU <sub>7</sub>	QS + HS
2538363.18	0.10	1.01	2025 EM	HS + QS
2584941.03	0.15	15.34	2025 FP	CP
2498021.74	0.18	5.46	2025 GL	CP
2421472.37	0.02	21.49	2025 QM <sub>9</sub>	CP
2415098.78	0.09	3.33	2025 UF <sub>5</sub>	HS + QS
2388483.65	0.26	2.17	2025 UK <sub>9</sub>	HS

Table A.2: Known asteroids sorted by their designations that are *not* Earth co-orbitals now but are, or will be, co-orbital at some other time in the range of years from 1600-2500. JD is the nearest Julian date to the current date that the object will have, or had, semi-major axis  $a = 1$ . The eccentricity,  $e$ , and inclination,  $i$  are provided at JD.